INTERNATIONAL JOURNAL OF ROBUST AND NONLINEAR CONTROL
Int. J. Robust Nonlinear Control 2002; **12**:207–242 (DOI: 10.1002/rnc.683)

Co-ordination and control of distributed spacecraft systems using convex optimization techniques

Michael Tillerson[1,†,¶], Gokhan Inalhan[2,‡,‖] and Jonathan P. How[1,*,§,**]

[1] *Department of Aeronautics and Astronautics, MIT, USA*
[2] *Department of Aeronautics and Astronautics, Stanford University, USA*

SUMMARY

Formation flying of multiple spacecraft is an enabling technology for many future space science missions. However, the co-ordination and control of these instruments poses many difficult design challenges. This paper presents fuel/time-optimal control algorithms for a co-ordination and control architecture that was designed for a fleet of spacecraft. This architecture includes low-level formation-keeping algorithms and a high-level fleet planner that creates trajectories to re-size or re-target the formation. The trajectory and formation-keeping optimization algorithms are based on the solutions of linear and integer programming problems. The result is a very flexible optimization framework that can be used off-line to analyse various aspects of the mission design and in real time as part of an onboard autonomous formation flying control system. The overall control approach is demonstrated using a nonlinear simulation environment that includes realistic measurement noises, disturbances, and actuator nonlinearities. Copyright © 2002 John Wiley & Sons, Ltd.

KEY WORDS: formation flying control; distributed spacecraft systems; real-time trajectory optimization; linear programming

1. INTRODUCTION

Formation flying of multiple spacecraft is an enabling technology for many future space science missions including enhanced stellar optical interferometers and virtual platforms for earth observations. This approach will use a distributed array of simple but highly co-ordinated microsatellites to form a 'virtual satellite bus' that replaces the standard monoliths used today

*Correspondence to: Jonathan P. How, Dept. of Aeronautics and Astronautics, MIT, U.S.A.
[†] Research Assistant
[‡] Research Assistant
[§] Associate Professor
[¶] E-mail: mike_t@mit.edu
[‖] E-mail: ginalhan@leland.stanford.edu
[**] E-mail: jhow@mit.edu

Contract/grant sponsor: AIR FORCE; contract/grant number: F49620-99-1-0095
Contract/grant sponsor: NASA GSFC; contract/grant number: NAG5-6233-0005

[1,2]. Strong interest in the formation flying concept has led to several planned and proposed space missions including: ST-3 and Terrestrial Planet Finder [3], EO-1 [4], TechSat-21 [5], and Orion-Emerald [6]. However, to achieve the goals of these future missions, many guidance, navigation and control challenges must be addressed. For example, very tight co-ordination, control, and monitoring of the distributed vehicles in the cluster will be required to achieve the stringent payload pointing requirements for a radar mission such as TechSat-21 [5].

Some of the key challenges in this problem are in the design of a fleet control architecture that can perform the high-level (mission management and planning to enable resource allocation across the fleet) and low-level (onboard sensing, autonomous closed-loop relative navigation, and attitude determination) tasks. The primary difficulties are that: (1) with a large fleet, the computational aspects of the sensing and control are complicated by the large information flow and amount of processing required; (2) the vehicles must work cooperatively to perform the science observations; (3) the differential disturbance environment and nonlinear actuator operations could be uncertain; and (4) the fleet must undergo both resizing and configuration change maneuvers.

The primary focus of most of the formation flying research to date has been to develop fuel-efficient methods of performing scientifically useful observations. In particular, much of the research for cluster dynamic modelling and control has focused on the design of *passive apertures*, which are (typically short baseline) periodic formation configurations that provide good, distributed, Earth imaging and reduce the tendency of the vehicles to drift apart [7]. These passive apertures can be designed using closed-form solutions provided by linearized orbital equations (e.g. Hill's equations for a circular reference orbit) [7–10]. A key aspect of the formation control in LEO is to maneuver the vehicles in the fleet to specified positions in one of these aperture, which is essentially a trajectory design and tracking problem. Of course, the goal is to optimize these trajectories so that the vehicles are accurately initialized in a reasonable amount of time using the least amount of fuel possible. With disturbance modelling errors, sensor noise, and actuator nonlinearities, this initialization will typically be imperfect, which will eventually cause the cluster to disperse. Thus, a combination of both feedforward and feedback control will be required to correct for these errors. Fuel optimized formation-keeping control will also be required to maintain the vehicles within a specified tolerance of their desired aperture locations.

The primary purpose of this paper is to present fuel-optimal control algorithms that can be used in the co-ordination and control architecture to address these trajectory design issues. These algorithms build on a core of real-time optimization based on the solution of several linear programming (LP) trajectory planning problems [11,12]. The approach uses the linearized orbital dynamics, which have been analysed to show that they provide precise models for short baseline formations (on the order of a few hundred meters) [7]. The LP approaches to formation-keeping, trajectory design, and fleet co-ordination are demonstrated using a commercially available, high-fidelity nonlinear orbit propagation tool [13]. The simulations include realistic disturbance models, measurement errors, and typical propulsion system nonlinearities such as finite thrust and minimum impulse bit. The simulation results indicate that noise in the relative velocity measurements could play a crucial role in the fleet performance and/or fuel cost. This paper provides a very flexible optimization framework that can be used before launch to analyse various aspects of the mission design and during flight as part of an onboard autonomous formation flying control system.

2. RELATIVE FORMATION DYNAMICS

The following presents the dynamics for the relative motion of a satellite with respect to a reference satellite on an eccentric orbit. These dynamics are later used in modelling multiple spacecraft co-ordination problems. Our brief but precise development of the equations of motion follows Reference [14], and the full details are available in References [15,16]. The location of each spacecraft within a formation is given by

$$\mathbf{R}_j = \mathbf{R}_{\mathrm{fc}} + \boldsymbol{\rho}_j \tag{1}$$

where $\mathbf{R}_{\mathrm{fc}}$ and $\boldsymbol{\rho}_j$ correspond to the location of the formation centre and the relative position of the jth spacecraft with respect to that point. The formation centre can either be fixed to an orbiting satellite, or just a local point that provides a convenient reference for linearization. The reference orbit in the earth centered inertial (ECI) reference frame is represented by the standard orbital elements $(a, e, i, \Omega, \omega, \theta)$, which correspond to the semi-major axis, eccentricity, inclination, right ascension of the ascending node, argument of periapsis and true anomaly.

With the assumption that $|\boldsymbol{\rho}_j| \ll |\mathbf{R}_{\mathrm{fc}}|$, the equations of motion of the jth spacecraft under the gravitational attraction of a main body

$${}_i\ddot{\mathbf{R}}_j = -\frac{\mu}{|\mathbf{R}_j|^3}\mathbf{R}_j + \mathbf{f}_j \tag{2}$$

can be linearized around the formation centre to give

$${}_i\ddot{\boldsymbol{\rho}}_j = -\frac{\mu}{|\mathbf{R}_{\mathrm{fc}}|^3}\left(\boldsymbol{\rho}_j - \frac{3\mathbf{R}_{\mathrm{fc}} \cdot \boldsymbol{\rho}_j}{|\mathbf{R}_{\mathrm{fc}}|^2}\mathbf{R}_{\mathrm{fc}}\right) + \mathbf{f}_j \tag{3}$$

where the accelerations associated with other attraction fields, disturbances or control inputs are included in $\mathbf{f}_j$. The derivatives in the ECI reference frame are identified by the preceding subscript i. A natural basis for inertial measurements and scientific observations is the orbiting (*non-inertial*) reference frame Σ_{c}, fixed to the formation centre (see Figure 1). Using kinematics, the relative acceleration observed in the inertial reference frame ${}_i\ddot{\boldsymbol{\rho}}_j$ can be related to the measurements in the orbiting reference frame

$${}_i\ddot{\boldsymbol{\rho}}_j = {}_c\ddot{\boldsymbol{\rho}}_j + 2{}_i\dot{\boldsymbol{\Theta}} \times {}_c\dot{\boldsymbol{\rho}}_j + {}_i\dot{\boldsymbol{\Theta}} \times ({}_i\dot{\boldsymbol{\Theta}} \times \boldsymbol{\rho}_j) + ({}_i\ddot{\boldsymbol{\Theta}} \times \boldsymbol{\rho}_j) \tag{4}$$

where ${}_i\dot{\boldsymbol{\Theta}}$ and ${}_i\ddot{\boldsymbol{\Theta}}$ correspond to the angular velocity and acceleration of this orbiting reference frame. The fundamental vectors $(\boldsymbol{\rho}_j, \mathbf{R}_{\mathrm{fc}}, {}_i\dot{\boldsymbol{\Theta}})$ in Equations (3) and (4) can be expressed in Σ_{c} as

$$\boldsymbol{\rho}_j = x_j\hat{k}_x + y_j\hat{k}_y + z_j\hat{k}_z \tag{5}$$

$$\mathbf{R}_{\mathrm{fc}} = R_{\mathrm{fc}}\hat{k}_x \tag{6}$$

$${}_i\dot{\boldsymbol{\Theta}} = \dot{\theta}\hat{k}_z \tag{7}$$

where the unit vector $\hat{k}_x$ points radially outward from Earth's centre (anti-nadir pointing) and $\hat{k}_y$ is in the in-track direction along increasing true anomaly. This right-handed reference frame is completed with $\hat{k}_z$, pointing in the cross-track direction. All of the proceeding vectors and their time rate of changes are expressed in the orbiting reference frame Σ_{c}.

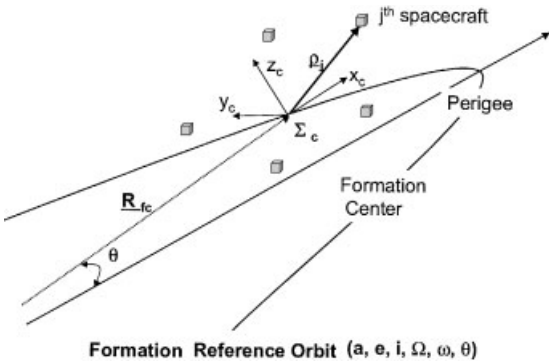

Figure 1. Relative motion in formation reference frame.

Combining Equations (3) and (4) to obtain an expression for ${}_c\ddot{\boldsymbol{\rho}}_j$, and using Equations (5)–(7), it is clear that the linearized relative dynamics with respect to an eccentric orbit can be expressed via a unique set of elements and their time rate of change. This set consists of the relative states $[x_j, y_j, z_j]$ of each satellite, the radius R_{fc} and the angular velocity $\dot{\theta}$ of the formation centre. Using fundamental orbital mechanics describing planetary motion [17,18], the radius and angular velocity of the formation centre can be written as

$$|\mathbf{R}_{\mathrm{fc}}| = \frac{a(1-e^2)}{1+e\cos\theta} \quad \text{and} \quad \dot{\theta} = \frac{n(1+e\cos\theta)^2}{(1-e^2)^{3/2}} \tag{8}$$

where $n = \sqrt{\mu/a^3}$ is the natural frequency of the reference orbit. These expressions can be substituted into the equation for ${}_c\ddot{\boldsymbol{\rho}}_j$ to obtain the relative motion of the jth satellite in the orbiting formation reference frame

$$\begin{aligned}\frac{\mathrm{d}}{\mathrm{d}t}\begin{bmatrix}\dot{x}\\ \dot{y}\\ \dot{z}\end{bmatrix}_j &= -2\begin{bmatrix}0 & -\dot{\theta} & 0\\ \dot{\theta} & 0 & 0\\ 0 & 0 & 0\end{bmatrix}\begin{bmatrix}\dot{x}\\ \dot{y}\\ \dot{z}\end{bmatrix}_j - \begin{bmatrix}-\dot{\theta}^2 & 0 & 0\\ 0 & -\dot{\theta}^2 & 0\\ 0 & 0 & 0\end{bmatrix}\begin{bmatrix}x\\ y\\ z\end{bmatrix}_j\\ &\quad - \begin{bmatrix}0 & -\ddot{\theta} & 0\\ \ddot{\theta} & 0 & 0\\ 0 & 0 & 0\end{bmatrix}\begin{bmatrix}x\\ y\\ z\end{bmatrix}_j + n^2\left(\frac{1+e\cos\theta}{1-e^2}\right)^3\begin{bmatrix}2x\\ -y\\ -z\end{bmatrix}_j + \begin{bmatrix}f_x\\ f_y\\ f_z\end{bmatrix}_j\end{aligned} \tag{9}$$

The terms on the right-hand side of this equation correspond to the Coriolis acceleration, centripetal acceleration, accelerating rotation of the reference frame, and the virtual gravity gradient terms with respect to the formation reference. The right-hand side also includes the combination of other external and control accelerations in $\mathbf{f}_j$. These terms can be explicitly presented for each spacecraft as

$$\begin{bmatrix}f_x\\ f_y\\ f_z\end{bmatrix}_j = \begin{bmatrix}u_x\\ u_y\\ u_z\end{bmatrix}_j + \begin{bmatrix}w_x\\ w_y\\ w_z\end{bmatrix}_j \tag{10}$$

where $u = [u_x(t)\ u_y(t)\ u_z(t)]^{\mathrm{T}} : \mathbb{R} \to \mathbb{R}^3$ represents the control inputs and $w = [w_x(t)\ w_y(t)\ w_z(t)]^{\mathrm{T}} : \mathbb{R} \to \mathbb{R}^3$ represents the combination of other external accelerations, such as dis turbances.

Note that care must be taken when interpreting and using the equations of motion and the relative states in a nonlinear analysis. The difficulty results from the linearization process, which maps the curvilinear space to a rectangular one via a small curvature approximation. In this case, a relative separation in the in-track direction in the linearized equations actually corresponds to an incremental phase difference in true anomaly, θ.

Although Equation (9) is expressed in the time domain, monotonically increasing true anomaly (θ) of the reference orbit provides a natural basis for parameterizing the fleet time and motion. This observation is based on the fact that the angular velocity and the radius describing the orbital motion are functions of the true anomaly [17]. Using θ as the free variable, the equations of motion can be transformed using the relationships

$$(\dot{\cdot}) = (\cdot)'\dot{\theta} \quad \text{and} \quad (\ddot{\cdot}) = (\cdot)''\dot{\theta}^2 + \dot{\theta}\dot{\theta}'(\cdot)' \tag{11}$$

With these transformations, the set of linear time-varying (LTV) equations describing the relative motion in an eccentric orbit can be written as

$$\begin{aligned}
\frac{\mathrm{d}}{\mathrm{d}\theta}\begin{bmatrix} x' \\ x \\ y' \\ y \end{bmatrix}_j &= \begin{bmatrix} \frac{2e\sin\theta}{1+e\cos\theta} & \frac{3+e\cos\theta}{1+e\cos\theta} & 2 & \frac{-2e\sin\theta}{1+e\cos\theta} \\ 1 & 0 & 0 & 0 \\ -2 & \frac{2e\sin\theta}{1+e\cos\theta} & \frac{2e\sin\theta}{1+e\cos\theta} & \frac{e\cos\theta}{1+e\cos\theta} \\ 0 & 0 & 1 & 0 \end{bmatrix}_j \begin{bmatrix} x' \\ x \\ y' \\ y \end{bmatrix}_j \\
&\quad + \frac{(1-e^2)^3}{(1+e\cos\theta)^4 n^2}\begin{bmatrix} 1 & 0 \\ 0 & 0 \\ 0 & 1 \\ 0 & 0 \end{bmatrix}\begin{bmatrix} u_x \\ u_y \end{bmatrix}_j \\
&\quad + \frac{(1-e^2)^3}{(1+e\cos\theta)^4 n^2}\begin{bmatrix} 1 & 0 \\ 0 & 0 \\ 0 & 1 \\ 0 & 0 \end{bmatrix}\begin{bmatrix} w_x \\ w_y \end{bmatrix}_j
\end{aligned} \tag{12}$$

$$\begin{aligned}
\frac{\mathrm{d}}{\mathrm{d}\theta}\begin{bmatrix} z' \\ z \end{bmatrix} &= \begin{bmatrix} \frac{2e\sin\theta}{1+e\cos\theta} & \frac{-1}{1+e\cos\theta} \\ 1 & 0 \end{bmatrix}_j \begin{bmatrix} z' \\ z \end{bmatrix}_j + \frac{(1-e^2)^3}{(1+e\cos\theta)^4 n^2}\begin{bmatrix} 1 \\ 0 \end{bmatrix} u_{zj} \\
&\quad + \frac{(1-e^2)^3}{(1+e\cos\theta)^4 n^2}\begin{bmatrix} 1 \\ 0 \end{bmatrix} w_{zj}
\end{aligned} \tag{13}$$

As shown, the in-plane (x, y) and out-of-plane (z) motions are decoupled (except where the disturbance models can create coupling) and can be expressed separately.

For a circular reference orbit, $e = 0$, substituting $\dot{\theta} = n_0$, $\ddot{\theta} = 0$, and transforming Equations (12) and (13) to time-domain results in the well-known Clohessy–Wiltshire or Hill's equations

$$\frac{\mathrm{d}}{\mathrm{d}t}\begin{bmatrix}\dot{x}\\ x\\ \dot{y}\\ y\\ \dot{z}\\ z\end{bmatrix} = \begin{bmatrix}0 & 3n_o^2 & 2n_o & 0 & 0 & 0\\ 1 & 0 & 0 & 0 & 0 & 0\\ -2n_o & 0 & 0 & 0 & 0 & 0\\ 0 & 0 & 1 & 0 & 0 & 0\\ 0 & 0 & 0 & 0 & 0 & -n_o^2\\ 0 & 0 & 0 & 0 & 1 & 0\end{bmatrix}\begin{bmatrix}\dot{x}\\ x\\ \dot{y}\\ y\\ \dot{z}\\ z\end{bmatrix} + \begin{bmatrix}1 & 0 & 0\\ 0 & 0 & 0\\ 0 & 1 & 0\\ 0 & 0 & 0\\ 0 & 0 & 1\\ 0 & 0 & 0\end{bmatrix}\begin{bmatrix}u_x\\ u_y\\ u_z\end{bmatrix} + \begin{bmatrix}1 & 0 & 0\\ 0 & 0 & 0\\ 0 & 1 & 0\\ 0 & 0 & 0\\ 0 & 0 & 1\\ 0 & 0 & 0\end{bmatrix}\begin{bmatrix}w_x\\ w_y\\ w_z\end{bmatrix} \tag{14}$$

Equations (12) and (13) can easily be transformed to time domain using the relationships in Equations (11). These new equations can be compactly represented as a general linear time-varying state-space model

$$\dot{x} = A(t)x(t) + B(t)u(t) + B_d(t)w(t) \tag{15}$$

These LTV equations will be used for the numerical analysis of the optimization algorithms.

The key reason for using the linear time-varying equations (Equations (12) and (13)), which are extensions of the standard Hill's equations, is described in detail in previous work [14]. In particular, Reference [14] shows through various analytic approximations and numerical simulations that the modelling errors associated with a circular reference orbit assumption can be a dominant error source when compared to other disturbances (such as differential J_2), even for orbits with low eccentricity, such as $e = 0.005$, which is typical of shuttle orbits. In addition, a key observation was that simple control systems that do not model the effects of eccentricity, process this error as a differential disturbance and thus work against the natural motion. This causes the controllers to continuously use fuel to correct for the modelling errors. However, accounting for these errors using the initialization method for eccentric orbits (as shown in Reference [10]) results in a considerable reduction in fuel cost.

The general state-space model given in Equation (15) can be discretized using the well-known technique of approximately integrating the dynamics in Equations (12), (13) or (14) over one sample period, T_s. Here A_k, B_k correspond to $A(kT_s)$ and $B(kT_s)$ for approximate integration. In the case of the Hill's equations, $A_k = A$ which is constant and $B_k = B$ which is constant. With the inclusion of the desired output and the direct transition matrices, the discretized relative

dynamics take the form [19]

$$x(k+1) \approx e^{A_k T_s} x(k) + \int_0^{T_s} e^{A_k \xi}\, d\xi\, B_k u(k) + \int_0^{T_s} e^{A_k \xi}\, d\xi\, B_{dk} w(k)$$
$$\Rightarrow x(k+1) = F_k x(k) + G_k u(k) + M_k w(k) \tag{16}$$

$$y(k) = H_k x(k) + J_k u(k) + P_k w(k), \quad t = kT_s \tag{17}$$

where the state transition and input matrices for control and disturbances correspond to

$$F_k = e^{A_k T_s}, \quad G_k = \int_0^{T_s} e^{A_k \xi}\, d\xi\, B_k, \quad M_k = \int_0^{T_s} e^{A_k \xi}\, d\xi\, B_{dk} \tag{18}$$

These equations are the basis of the control and co-ordination design in the following sections. This analysis will focuses on the relative states, i.e. relative position and velocities of the vehicles. Thus typically $J_k = 0$, $P_k = 0$, and H_k is of the form

$$H_k = \begin{bmatrix} [1 & \cdots & \cdots] & \cdots & [-1 & \cdots & \cdots] & 0 & 0 & 0 \\ [1 & \cdots & \cdots] & \cdots & [0 & -1 & \cdots] & 0 & 0 & 0 \\ & \vdots & & \vdots & & \vdots & & \vdots & \vdots & \vdots \\ [0 & 1 & \cdots] & \cdots & [0 & -1 & \cdots] & 0 & 0 & 0 \\ & \vdots & & \vdots & & \vdots & & \vdots & \vdots & \vdots \end{bmatrix} \tag{19}$$

which extracts and differences specific parts of the position and velocity states associated with the N vehicles in the fleet. The next section gives the computational form of these dynamic equations that will be used in the optimization.

Remark 1

The time-step, T_s, is typically chosen to be small (i.e. on the order of 5.4 s so that there are 1000 points per orbit) to obtain an accurate discretization. However, this results in a large number of inputs and constraints for the trajectory optimization, which can take several minutes to solve. One method to reduce these computational times for a real-time implementation is to only allow inputs every m-(integer) time-steps and/or only enforcing the constraints every p-(integer) time-steps. For example, with $m = p = 10$, this greatly reduces the size of the optimization problem, resulting in solution times on the order of seconds. This decreased solution time is obtained at the expense of system performance because the control inputs are allowed less often (reduces efficiency) and the position constraints are only tested at certain time-steps (violations are possible at intermediate time-steps). However, as discussed in more detail in Reference [20], these m and p parameters provide a direct means for tuning the system to trade-off performance for reduced computational effort.

3. GENERAL SYSTEM DESCRIPTION

The previous section presented the linearized relative spacecraft dynamics in a linear time-varying form (see Equations (16) and (17)) where $x(k) \in R^n$ are the states, $u(k) \in R^m$

are control inputs, and $w(k) \in R^p$ are the differential disturbances acting on the vehicles. The disturbances are typically modelled as acting on each spacecraft as differential with respect to the formation centre represented either by another vehicle or a general point on the reference orbit. The vector $y(k) \in R^l$ corresponds to the measured outputs or the variables of interest to the control design. The output $y(k)$ can be calculated using discrete convolution of the form

$$\begin{aligned} y(k) &= H_k F^{(k,k)} x(0) + [J_k u(k) + P_k w(k)] \\ &\quad + \sum_{i=0}^{k-1} H_k F^{(k-i-1,k)} [G_i u(i) + M_i w(i)], \quad k \geqslant 1 \end{aligned} \tag{20}$$

where $F^{(j,k)}$ corresponds to

$$F^{(j,k)} = \begin{cases} F_{(k-1)} \cdots F_{(k-j+1)} F_{(k-j)}, & 2 \leqslant j \leqslant k \\ F_{(k-1)}, & j = 1 \\ I, & j = 0 \end{cases} \tag{21}$$

Note that if the fleet has a circular reference orbit, then the system matrices ($F_k, G_k, H_k, J_k, M_k, P_k$) will be independent of time and $F^{(k-i-1,k)}$ simply corresponds to F^{k-i-1}. Equation (20) has the simple matrix representation

$$y(k) = A(k) U_k + b(k) \tag{22}$$

where $A(k)$ and $b(k)$ are given by

$$A(k) = [H_k F^{(k-1,k)} G_0 \quad H_k F^{(k-2,k)} G_1 \quad \ldots \quad H_k F^{(0,k)} G_{k-1} \quad J_k] \tag{23}$$

$$\begin{aligned} b(k) = &[H_k F^{(k-1,k)} M_0 \quad H_k F^{(k-2,k)} M_1 \quad \cdots \quad H_k F^{(0,k)} M_{k-1} \quad P_k] \begin{bmatrix} w(0) \\ w(1) \\ \vdots \\ w(k) \end{bmatrix} \\ &+ H_k F^{(k,k)} x(0) \end{aligned} \tag{24}$$

$H_k F^{(k-i,k)} G_0$ is the pulse response of the system, and

$$U_k = [u(0)^{\mathrm{T}} \quad u(1)^{\mathrm{T}} \quad \ldots \quad \ldots \quad u(k-1)^{\mathrm{T}} \quad u(k)^{\mathrm{T}}]^{\mathrm{T}} \tag{25}$$

This affine plant description is the basis of the following trajectory and control design. The next section introduces unique system limitations, such as state-space constraints, actuator saturation and slew rates to the formation co-ordination problem. These will ensure that the optimal control schemes are feasible for each element of the distributed system.

4. BASIC FORMATION PLANNING

This section presents the formulation of the basic trajectory planning problem as an LP optimization [21,22]. There are two primary trajectory design problems of interest for formation flying spacecraft:

1. Formation initialization or reconfiguration problem.
2. Formation-keeping problem.

Based on the affine system model in Equation (22), the general formation initialization or reconfiguration control problem is to locate the N vehicles in the fleet at the desired relative positions with the desired relative velocities after n time-steps, while minimizing a weighted sum ($c_j \geqslant 0$) of the $\|\cdot\|_1$ norm of the control inputs by each spacecraft. The objective statement is

$$\min_{U_n} \sum_{j=1}^{m} c_j \|u_j\|_1 \quad \text{subject to } y(n) = y_{\text{des}}(n) \tag{26}$$

where $u_j = [u_j(0)\ u_j(1)\ \ldots\ u_j(n)]^{\mathrm{T}}$ is the fuel used by the jth thruster on the spacecraft. Equation (26) is the cost function used to design trajectories for a single spacecraft. Note that the trajectory design could be performed simultaneously for the entire fleet by extending the cost in Equation (26) to include all control inputs for all spacecraft. The fleet-level trajectory optimization is discussed in detail in Section 5.

The objective of the formation-keeping control problem is to use the minimum control effort necessary to maintain the vehicle to within some tolerance of a specified desired set of co-ordinates at each time-step k. The performance specification is represented by a 'slab',

$$\begin{aligned} &|y_j(k) - y_{j\text{des}}(k)| \leqslant \varepsilon_j, \quad \varepsilon_j \geqslant 0 \\ &\Rightarrow -\varepsilon_j \leqslant y_j(k) - y_{j\text{des}}(k) \leqslant \varepsilon_j \quad \forall j = 1, \ldots, l \end{aligned} \tag{27}$$

where ε_j is the error bound associated with each co-ordinate y_j. For example, these bounds are specified by the error box, e.g. separation of ± 10 m in-track, ± 5 m radial, and ± 10 m cross-track. Formation-keeping under differential disturbances is achieved by placing constraints on the position of the spacecraft relative to the desired co-ordinates, which corresponds to the centre of the error box. Note that the centre of each error box is referenced to the formation centre, which could be a set of reference orbital elements or another spacecraft.

Remark 2

$y_{\text{des}}(n)$ in Equation (26) can represent the states $x(n)$ directly or any affine relationship between the states, such as the constraint $S(n)y_{\text{des}}(n) \leqslant T(n)$. This more general form can be used to place constraints on only part of the system state. For example, one important problem [10] is to control a group of spacecraft so that they have the same energy level, which tends to reduce the rate that they will drift apart. This type of energy constraint can be written as

$$\dot{y}_j + 2n_o x_j = c, \quad \forall j \text{ spacecraft}$$

where c is an arbitrary, but common, constant. Note that this process does not specify any fixed values for the relative states such as radial position, x_j or in-track velocity, $\dot{y}_j$.

4.1. Additional constraints

Equation (26) is the basic form of the general formation control problems, but other constraints must be included to address the following issues:

1. The formation-keeping requires that the state variables (co-ordinates) be constrained at each time-step to ensure that the vehicles stay with a specified tolerance of the desired location.
2. The thrust levels of each actuator on each spacecraft typically have unique bounds that must be correctly addressed in the optimization to obtain precise formation flying.
3. For spacecraft utilizing micro-propulsion, large maneuvers require long periods of thruster firings and an impulsive ΔV assumption does not hold for these transfers.
4. Some actuation methods have a very slow slew rate (such as drag panels), and this must be accounted for in the control design.

This section demonstrates how to include these constraints and presents solutions to several other problems typically encountered in formation co-ordination and control (see Section 6 for details and examples).

The different aspects observed in these examples can be structured into a standard format that can easily be included in the basic optimization problem given previously:

- *State-space constraints* are described via

$$S(k)y(k) \leqslant T(k) \quad \forall k \in \{0, 1, \ldots, n\} \tag{28}$$

  which can be written as a function of the control input sequence using Equation (22)

$$[S(k)A(k)]U(k) \leqslant [T(k) - S(k)b(k)] \quad \forall k \in \{0, 1, \ldots, n\} \tag{29}$$

  These equations can be combined into the general inequality

$$\bar{S}U_n \leqslant \bar{T} \tag{30}$$

- *Control input saturation* is described via

$$u_j^{\min}(i) \leqslant u_j(i) \leqslant u_j^{\max}(i) \tag{31}$$

  which can be written in a compact form for n steps using the previous definition of U_n

$$\begin{bmatrix} I \\ -I \end{bmatrix} U_n \leqslant \begin{bmatrix} U_n^{\max} \\ -U_n^{\min} \end{bmatrix} \tag{32}$$

  Note that typically $u^{\min} = -u^{\max}$.
- *Actuator rate limits* described as

$$r_j^{\min}(i) \leqslant u_j(i+1) - u_j(i) \leqslant r_j^{\max}(i) \tag{33}$$

also can be expressed in the compact form

$$\begin{bmatrix} v_n \\ -v_n \end{bmatrix} U_n \leqslant \begin{bmatrix} R_n^{\max} \\ -R_n^{\min} \end{bmatrix} \tag{34}$$

where

$$v_n = \begin{bmatrix} -1 & \cdots & 1 & \cdots & \cdots & \cdots \\ & -1 & \cdots & 1 & & \\ & & \ddots & & \ddots & \\ \cdots & \cdots & \cdots & -1 & \cdots & 1 \end{bmatrix} \tag{35}$$

The inequality constraints involving the control input set U_n can be combined with state-space constraints to form the inequality

$$\begin{bmatrix} I \\ -I \\ v_n \\ -v_n \\ \bar{S} \end{bmatrix} U_n \leqslant \begin{bmatrix} U_n^{\max} \\ -U_n^{\min} \\ R_n^{\max} \\ -R_n^{\min} \\ \bar{T} \end{bmatrix} \quad \text{or} \quad \Gamma_n U_n \leqslant \beta_n \tag{36}$$

With the addition of these constraints, the formation initialization control problem in Equation (26) can be written as

$$\mathrm{J}_{\mathrm{sp}}^{\star} = \min_{U_n} \sum_{j=1}^{m} c_j \|u_j\|_1 \tag{37}$$

$$\text{subject to} \quad \begin{matrix} y_{\mathrm{des}}(n) = A(n)U_n + b(n) \\ \Gamma_n U_n \leqslant \beta_n \end{matrix} \tag{38}$$

4.2. Linear program formulation

To rewrite the formation control problem as a linear program, two slack variables are introduced that define the positive and negative parts of the control [21,22] input

$$U_n = U_n^+ - U_n^-, \quad U_n^+ \geqslant 0, \ U_n^- \geqslant 0 \tag{39}$$

Using c_{ij} as the weight for the input from the jth actuator at the ith time-step, define $C^{\mathrm{T}} = [c_{00}\ c_{01}\ \ldots\ c_{nm}\ c_{00}\ c_{01} \ldots\ c_{nm}]$ as the weights (typically all set to 1) on each of the positive and negative parts of the control inputs.

The formation initialization and reconfiguration problem can then be rewritten as the standard linear program

$$J^*_{sp-lp} = \min_{\hat{U}_n} C^T \hat{U}_n \tag{40}$$

$$\text{subject to} \quad \begin{cases} [A(n) \quad -A(n)]\hat{U}_n = y_{des}(n) - b(n) \\ \begin{bmatrix} \Gamma_n & -\Gamma_n \\ -I & 0 \\ 0 & -I \end{bmatrix} \hat{U}_n \leqslant \begin{bmatrix} \beta_n \\ 0 \\ 0 \end{bmatrix} \\ \hat{U}_n = \begin{bmatrix} U_n^+ \\ U_n^- \end{bmatrix} \end{cases} \tag{41}$$

As given in the structure of the problem, the information necessary to complete the co-ordination problem are the initial states x_0, the desired goal $y(n)$, and the system limitations embedded in the inequality constraints.

Remark 3
The formation-keeping control problem is formulated by replacing the terminal equality constraint with inequality constraints at each time-step k to constrain the state to be within some tolerance, y_{tol}

$$\begin{bmatrix} A(k) & -A(k) \\ -A(k) & A(k) \end{bmatrix} \hat{U}_k \leqslant \begin{bmatrix} y_{des}(k) - b(k) + y_{tol} \\ -y_{des}(k) + b(k) + y_{tol} \end{bmatrix} \tag{42}$$

The equality constraint given in Equation (41) can also readily be replaced with an inequality constraint of this form with $k = n$.

Remark 4
It can easily be shown that the LP cost in Equation (40) is equivalent to the $\|\cdot\|_1$ in Equation (37). For example, given an optimal command $u_k^\star$ at the kth time-step, the LP problem essentially solves the following optimization:

$$\min_{u_k^+, u_k^-} u_k^+ + u_k^-, \quad \text{subject to } u_k^+ - u_k^- = u_k^\star, \quad u_k^+ \geqslant 0, \; u_k^- \geqslant 0 \tag{43}$$

The optimal answer to this problem is (i) $u_k^+ = u_k^\star$, $u_k^- = 0$ if $u_k^\star \geqslant 0$ or (ii) $u_k^+ = 0$, $u_k^- = -u_k^\star$ if $u_k^\star < 0$. Thus the cost function $u_k^+ + u_k^-$ is equivalent to $|u_k^\star|$, as specified in the standard optimization in Equation (37). Of course, the LP optimization actually solves for u_k^+, u_k^- not $u_k^\star$.

The LP in Equations (40) and (41) can be solved very efficiently using many free and commercially available optimization programs [23–25]. The convexity of the LP problem essentially means that, if it exists, the solution result will be the global optimum. Thus, under these given dynamics, constraints, and cost assumptions, no other co-ordination or control method will outperform the LP solution. Another benefit of the LP approach is that the solution time increases slowly as the number of variables grows, which is true for all convex optimization problems.

4.3. *Effects of initial state uncertainty—robust LP approach*

As a result of estimation process associated with the relative navigation [26,27], it is expected that there will be an uncertainty associated with the current positions and velocities (initial states in the trajectory optimization). A key question that arises for any trajectory generation process is the effect of uncertainty in the initial state knowledge on the optimal plan. This subsection presents a simple technique to add robustness in the planning process to these uncertainties.

Uncertainty in the initial conditions can be addressed by developing a trajectory design that is robust to errors in $x(0)$. Based on the 'multiple-model' techniques successfully used for robust feedback control design [28,29], one approach to increasing robustness in the trajectory planner is to design the input sequence to simultaneously satisfy the constraints for several (m_{ic}) initial conditions. Note that, as shown in Equation (24), the initial condition only enters the problem though the righthand side $b(k)$. Thus in the general formulation given in Equations (26), the first constraint would be written in the form

$$[-A(k) \quad A(k)][\hat{U}_n] \leqslant y_{\text{des}}(k) - b_i(k) \quad \forall i = 1, \ldots, m_{\text{ic}} \tag{44}$$

where $b_i(k)$ from Equation (24) captures the response associated with each of the initial conditions $x_i(0)$.

To avoid adding a large number of constraints to the LP problem, these m_{ic} constraints can be replaced with a single constraint

$$[-A(k) \quad A(k)][\hat{U}_n] \leqslant y_{\text{des}}(k) - b_{\max}(k) \tag{45}$$

where $b_{\max}$ is formed using the following. Form the matrix B

$$B = [b_1 \quad \cdots \quad b_{m_{\text{ic}}}] \tag{46}$$

whose columns are the b_i vectors associated with each initial condition. Then determine the vector $b_{\max}$, the ith element of which is given by

$$b_{\max}(i) = \max_j B_{ij}, \quad \forall i = 1, \ldots, N \tag{47}$$

Because the approach typically only considers several ($m_{\text{ic}} = 1$–10) perturbed initial conditions, it is not guaranteed to provide an input sequence that will not violate the specified constraints. However, as with the robust feedback control design, experience indicates that the results from this approach are much less sensitive to errors in the initial conditions. This reduced sensitivity is clearly demonstrated in the examples presented in Section 6.2.1. Additional analysis of the effects of sensor noise on the LP control approach is available in Reference [30]. Future work will compare this 'multiple-model' approach to robustness with the guaranteed techniques in Reference [31].

4.4. *Soft constraints—always feasible solutions*

One difficulty that arises in using the LP approach to solve the spacecraft control problems is that the optimization might determine that the solution is infeasible. This most often occurs when, for the given system characteristics, the desired goals cannot be satisfied in the n steps of the plan. Another form of infeasibility arises due to the uncertainty in the initial conditions. For a given uncertainty and plan length, the objective of the control in this case is to maintain a desired position to within some tolerance. However, the variation in the plans developed for the initial conditions considered (see Section 4.3) could exceed the maximum tolerance, thereby

resulting in an infeasible solution. A bisection algorithm can be used to check feasibility for various time lengths, which will find a feasible solution, if it exists. However for real-time applications, it is important that the technique be capable of always providing feasible solutions to the problem.

An alternative approach is to include a tolerance, y_{tol}, on the terminal constraint for the reconfiguration problem, or state tolerance constraint for formation-keeping problem, and a scaling variable y_{scale} in the LP formulation such that

$$|y(k) - y_{\text{des}}(k)| \leqslant y_{\text{tol}} y_{\text{scale}} \quad \forall k = 1, \ldots, n \tag{48}$$

The modified problem formulation is then as follows:

$$\mathrm{J}^{*}_{\text{sc-lp}} = \min[C^{\mathrm{T}} \quad \phi] \begin{bmatrix} \hat{U}_n \\ y_{\text{scale}} \end{bmatrix} \tag{49}$$

$$\text{subject to} \quad \begin{cases} \begin{bmatrix} A(k) & -A(k) & -y_{\text{tol}} \\ -A(k) & A(k) & -y_{\text{tol}} \end{bmatrix} \begin{bmatrix} \hat{U}_k \\ y_{\text{scale}} \end{bmatrix} \leqslant \begin{bmatrix} y_{\text{des}}(k) - b(k) \\ -y_{\text{des}}(k) + b(k) \end{bmatrix} & \forall k = 1, \ldots, n \\ \begin{bmatrix} -I & 0 & 0 \\ 0 & -I & 0 \\ 0 & 0 & -I \end{bmatrix} \begin{bmatrix} \hat{U}_n \\ y_{\text{scale}} \end{bmatrix} \leqslant \begin{bmatrix} 0 \\ 0 \\ -1 \end{bmatrix} \\ \hat{U}_n = \begin{bmatrix} U_n^{+} \\ U_n^{-} \end{bmatrix} \end{cases} \tag{50}$$

where k represents each time-step and $k = n$ for the terminal time. The scaling variable, $y_{\text{scale}} \geqslant 1$, is heavily weighted in the cost function by $\phi \gg 1$ to prevent increasing the error box to achieve a solution with zero control inputs. Thus y_{scale} would only be increased to scale the error box if necessary to obtain a feasible solution. The scaling variable is also constrained to be greater than one to prevent reducing the position tolerance below the original size in an attempt to minimize the heavily weighted scaling variable at the expense of increasing the control input.

The relaxation process can also be used in a more general form for the inequality constraints $\Gamma_n U_n \leqslant \beta_n$ in Equation (36) by introducing a set of vectors v_n so that

$$\Gamma_n U_n - \beta_n \leqslant v_n \tag{51}$$

where $v_n = v_n^{+} - v_n^{-}$ with $v_n^{+} \geqslant 0$, $v_n^{-} \geqslant 0$. Here the inequality constraints are relaxed when the $v_n \geqslant 0$, so only the positive part of v_n, v_n^{+}, is required. The error in the inequality constraints is added to the cost function with a weight vector $\psi > 0$ on v_n^{+}. The optimization for the terminal

constraint then takes the following form:

$$\mathrm{J}^{*}_{\mathrm{scg-lp}} = \min[C^{\mathrm{T}} \quad \phi \quad \psi] \begin{bmatrix} \hat{U}_n \\ y_{\mathrm{scale}} \\ v_n^{+} \end{bmatrix} \tag{52}$$

$$\text{subject to} \begin{cases} \begin{bmatrix} A(k) & -A(k) & -y_{\mathrm{tol}} & 0 \\ -A(k) & A(k) & -y_{\mathrm{tol}} & 0 \end{bmatrix} \begin{bmatrix} \hat{U}_n \\ y_{\mathrm{scale}} \\ v_n^{+} \end{bmatrix} \leqslant \begin{bmatrix} y_{\mathrm{des}}(k) - b(k) \\ -y_{\mathrm{des}}(k) + b(k) \end{bmatrix} \\ \forall k = 1, \ldots, n \\ \begin{bmatrix} \Gamma_n & -\Gamma_n & 0 & -I \\ -I & 0 & 0 & 0 \\ 0 & -I & 0 & 0 \\ 0 & 0 & -I & 0 \\ 0 & 0 & 0 & -I \end{bmatrix} \begin{bmatrix} \hat{U}_n \\ y_{\mathrm{scale}} \\ v_n^{+} \end{bmatrix} \leqslant \begin{bmatrix} \beta_n \\ -1 \\ 0 \end{bmatrix} \\ \hat{U}_n = \begin{bmatrix} U_n^{+} \\ U_n^{-} \end{bmatrix} \end{cases} \tag{53}$$

Note that the dimension of the error vector could be reduced in this formulation because most problems are only concerned with the l_∞ norm of the error vector. Within the general structure presented above, this corresponds to replacing the vector variable v_n in Equation (52) with just a scalar v. In this case the inequalities are bounded by the worst case errors described v. The methods of creating always feasible solutions presented in Equations (50) and (52) can also be combined with a weighting in the cost function to balance the relaxation of the various constraints.

The LP problem formulation combined with the additional constraints, robustness, and feasibility methods provides an effective means of producing fuel-optimal trajectories for spacecraft. The LP problem can be solved independently for each spacecraft, allowing distribution of the computational load. However, the following section describes a method of co-ordinating the trajectory optimizations for the spacecraft to improve the fuel cost for the fleet.

5. CO-ORDINATION ALGORITHMS

With a large number of vehicles, the computational aspects of the fleet trajectory planning are complicated by the large information flow and the amount of processing required. This computational load can be balanced by distributing the effort over the fleet using a bidding process [32,33]. For example, in a typical formation flying scenario [2,7], the vehicles will be arranged as part of a *passive aperture*. These apertures provide relatively stable configurations that do not require as much fuel to perform the science observations. But changing the viewing mode of the fleet could require that the formation change configuration, moving from one aperture to another. In this case it is essential to find fuel- and time-efficient ways to move each

spacecraft to their locations in the new aperture, which is a challenging optimization problem with many possible final configurations.

The following describes a distributed solution to this problem, which builds on the results of References [32,33]. The approach partially alleviates the computational difficulties associated with solving the aperture optimization problem by distributing the effort over the entire fleet, and then using a co-ordinator to recombine the results. In this approach, the satellites analyse the possible final locations in a discrete set of global configurations and associate a cost with each. The linear programming tools in Section 4 are used to compute the fuel costs (and trajectories) to move each spacecraft from their current location to each possible final location. These simple calculations can be done in parallel by each spacecraft. The result is a list of predicted fuel costs for every possible final location (called a ΔV map), which are used to generate the fuel cost to move the fleet to each global configuration. These costs are based on fuel usage, but they could include other factors, such as the vehicle health.

Note that, in the placement of the formation around the passive aperture, the only requirement is that the vehicles be evenly spaced. Because the spacecraft are assumed to be identical, their ordering around the aperture is not important, so this corresponds to an assignment problem. In addition, the rotation of the entire formation around the aperture is not important. Each rotation angle of the formation around the ellipse corresponds to what is called a 'global configuration'. To consider only a discrete set of configurations, the aperture is typically discretized at 5° intervals. The ΔV maps are given to a centralized co-ordinator to perform the assignment process, which can be done in a number of ways.

To consider this assignment process in more detail, start by selecting one of the possible locations on the closed-form aperture, and then the $N-1$ equally spaced locations from that point. The N columns corresponding to these locations are then extracted from the overall ΔV map to form the $N \times N$ matrix

$$F = \begin{bmatrix} f_{11} & f_{12} & \cdots & f_{1N} \\ f_{21} & f_{22} & \cdots & f_{2N} \\ \vdots & & \ddots & \\ f_{N1} & \cdots & \cdots & f_{NN} \end{bmatrix} = [f_1 \quad f_2 \quad \cdots \quad f_N] \tag{54}$$

the elements (f_{ij}) of which are the fuel cost for the ith satellite to relocate to the jth position.

The following heuristic, which is based on the results of numerous examples, provides one way to solve the co-ordinator's assignment problem. The approach is to determine which position, on average, would require the most fuel to fill. This fuel cost is calculated by simply summing the ΔVs for each position. The location with the highest fuel total is then filled first by selecting the vehicle that requires the minimum amount of fuel to reach that position. The procedure is repeated until all positions are filled.

Algorithm

Initialize $I = [1 \ \cdots \ N]$ and $J = [1 \ \cdots \ N]$

Step 1: Find $j^\star = \arg\max_{j \in J} \sum_{i \in I} f_{ij}$

Step 2: Find $i^\star = \arg\min_{i \in I} f_{ij^\star}$

Step 3: Remove $i^\star$ from I and $j^\star$ from J: $I \rightarrow I \backslash \{i^\star\}$, $J \rightarrow J \backslash \{j^\star\}$.

Step 4: Remove the $i^\star$ row and $j^\star$ column from F and return to step 1.

This heuristic algorithm is typically used to reduce the problem until only three satellites (and three positions) remain. The six remaining scenarios can easily be examined to determine the best-possible configuration. This heuristic algorithm can be computed very quickly, but it typically does not provide the optimal solution. However, experience has shown that it is very good at avoiding poor configurations, and thus provides a viable solution approach.

The co-ordinator's assignment problem can also be solved using integer programming (IP) techniques [34–37]. Define the $N \times N$ matrix Y, the elements y_{ij} of which are binary and can be used to include logical conditions in the optimization. For example, $y_{ij} = 1$ would correspond to the ith satellite being located at the jth position on the aperture (and $y_{ij} = 0$ would mean that it is not):

$$Y = \begin{bmatrix} y_{11} & y_{12} & \cdots & y_{1N} \\ y_{21} & y_{22} & \cdots & y_{2N} \\ \vdots & & \ddots & \\ y_{N1} & \cdots & \cdots & y_{NN} \end{bmatrix} = [y_1 \quad y_2 \quad \cdots \quad y_N] \tag{55}$$

With the vectors

$$\tilde{F} = [f_1^{\mathrm{T}} \quad f_2^{\mathrm{T}} \quad \cdots \quad f_N^{\mathrm{T}}], \quad \tilde{Y} = \begin{bmatrix} y_1 \\ \vdots \\ y_N \end{bmatrix} \tag{56}$$

then the assignment problem for the co-ordinator can be written as

$$\mathrm{J}^{\star}_{\mathrm{co-ord}} = \min_{\tilde{Y}} \tilde{F}\tilde{Y} \tag{57}$$

$$\text{subject to} \quad \begin{array}{l} \sum_{i=1}^{N} y_{ij} = 1, \quad \forall j = 1, \ldots, N \\ \sum_{j=1}^{N} y_{ij} = 1, \quad \forall i = 1, \ldots, N \\ y_{ij} \in \{0, 1\} \quad \forall i, j \end{array} \tag{58}$$

Note that $\tilde{F}\tilde{Y}$ calculates the fuel cost associated with each configuration, and the co-ordinator selects the configuration that minimizes the total fuel cost for the fleet. The two summation constraints ensure that each satellite is given a location and that only one vehicle is placed at each location (an *exclusive or* condition) [34–37]. The selection algorithm can be modified to include the initial fuel conditions of each vehicle by simply adding the initial fuel state to the corresponding row of the ΔV map. Fuel balancing across the fleet can be addressed by weighting each row of the ΔV map by a factor $\alpha_i = \Delta V_{\mathrm{i0}}/\Delta V_{\mathrm{avg0}}$, where ΔV_{i0} is the initial fuel used by the ith spacecraft and ΔV_{avg0} is the average initial fuel used by the entire fleet. By design $\alpha_i > 1$ for vehicles that have used more fuel than the average, which tends to penalize their additional fuel expenditures more heavily.

The formation co-ordinator approach was applied to a reconfiguration example with eight vehicles. The vehicles start on one aperture (100 m semi-major axis) and recombine on a second one (200 m semi-major axis), see Figure 2. The maneuver also changes the orientation of the cross-track motion. The only hard constraint on the planning process is that the vehicles be placed with equal phasing on the new aperture. The cost maps for the satellites are based on

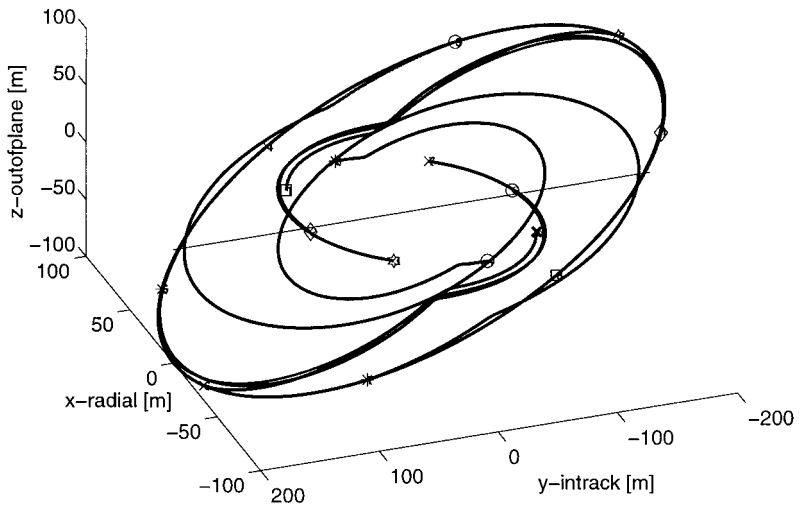

Figure 2. Hill's frame showing the optimized trajectories followed by the spacecraft to reconfigure the aperture.

their predicted fuel usage vs aperture location, and are shown in Figure 3. The circles in the figure show which location each vehicle was given in the fleet-optimal configuration. As is evident from the figure, all of the spacecraft received solutions that are close to the locations that would minimize their predicted fuel cost (all spacecraft are within 4 per cent of their minima, and four are within 2 per cent). However, it is also clear that two of the vehicles (#1 and #5) are forced to expend more fuel than the others, and two others (#2 and #6) are forced to select locations that are much higher compared to their fuel-optimal choices (4 per cent above). This is an example of a case where the team objectives and individual control objectives are in conflict, and sacrifices by some team members are required to obtain better overall performance.

For this example, the integer optimization takes approximately 1 s to solve using Matlab code [38] on a Pentium III (500 MHz). The heuristic algorithm takes significantly less time ($\leqslant 0.1$ s), and in this case, gave the same answer. Note that Reference [39] shows that the linear assignment problem can also be solved using linear programming with equality constraints, which in this example takes approximately 0.17 s. Figure 4 compares the fuel cost associated with the $(360/5)/8 = 9$ best configurations (there is an N-fold symmetry in the selection process). The ($\diamond$)'s show the costs associated with 800 other cases that were investigated for each configuration. These results show that some aperture configurations have a fuel cost that is 33 per cent higher than the optimal one given above.

With the discretization of the target aperture, this process is not guaranteed to be globally optimal, but this hierarchical approach offers some key benefits in that it:

1. Distributes the computational effort of the reconfiguration optimization since most calculations are done in parallel on much smaller-sized (LP and IP) problems.
2. Provides a simple method of finding optimized solutions that are consistent with the global constraints since the centralized co-ordinator determines the final solution.

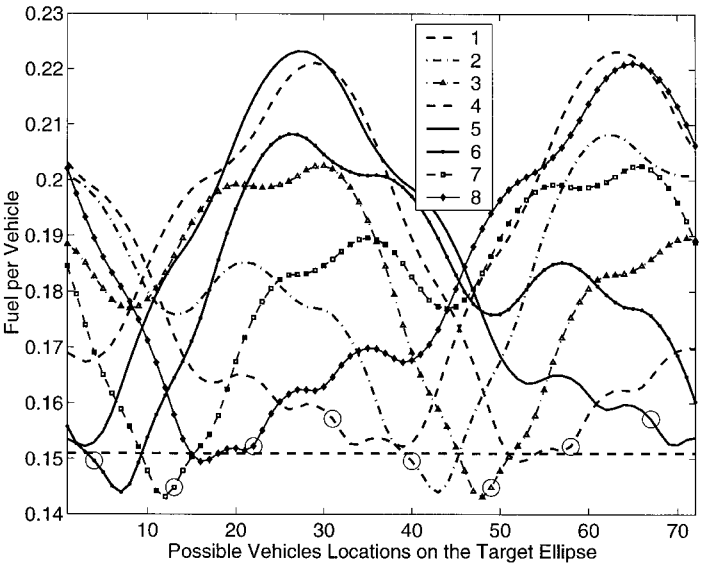

Figure 3. Associated predictions of the ΔV fuel cost to move to each location on the target aperture. Uses a 5° discretization of the target ellipse.

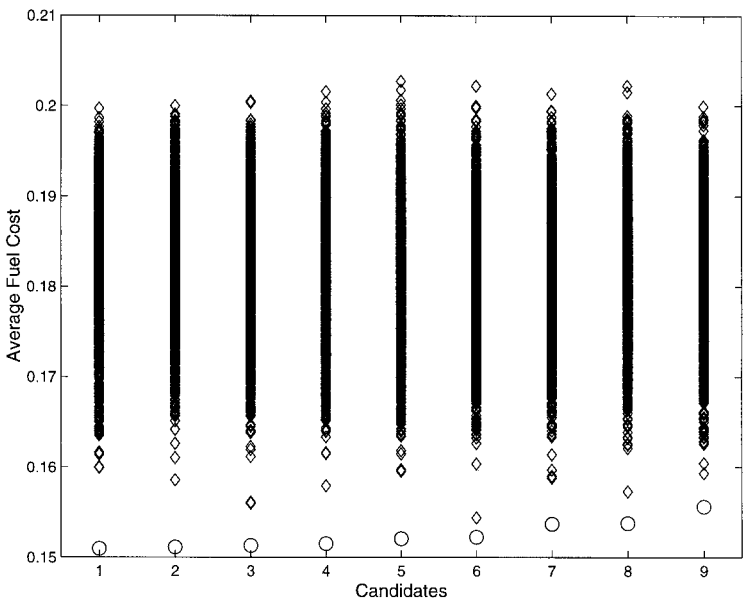

Figure 4. Comparison of the nine best alternative fleet configurations. The final design is #1. The (◇) symbols show 800 alternatives for each possible configuration.

3. Allows the vehicles to include individual decision models (e.g. bidding highly for a maneuver that requires less reorientation if there is a reaction wheel failure).

While the heuristic approach is faster to compute on this simple example, the advantage of the integer optimization approach to the co-ordination is that it enables the trajectory design and target aperture assignment to be combined into one centralized algorithm [36, 37]. This allows the co-ordinator to explicitly include additional constraints, such as collision avoidance and plume impingement, in the optimization. The technique has been demonstrated on small fleets (e.g. $N = 3$), and further extensions are under investigation.

6. SIMULATIONS

The satellite formation control problem consists of two types of maneuvers, a formation initialization or reconfiguration maneuver and a formation-keeping maneuver. Each of these types of maneuvers has two primary issues in the control problem. The first issue involves the selection of the dynamics used to determine the desired relative state of each satellite within the formation. The second issue is to determine how to control the satellite to achieve and maintain the specified desired state. Both parts of the control problem are discussed below.

The first issue is what relative dynamics and initialization procedure should be used to specify the desired state for obtaining or maintaining a passive aperture. For the formation initialization or reconfiguration maneuver, the desired state represents the terminal constraint in the control problem. For the formation-keeping maneuver the desired state is the position and velocity the satellite must maintain throughout the maneuvers. The desired state can be something as simple as an in-track separation or a more complicated case, such as a time-varying position on a passive aperture. Figure 5 shows an example of this second case—the desired state is given by the diamond and the position on the reference orbit is given by the circle. The reference orbit can be specified by one satellite in the formation, the formation centre, or a virtual satellite that is propagated with the formation. Typical periodic relative motion for a passive aperture in the absence of disturbances is also shown in Figure 5. The appropriate method for determining the desired relative state for passive apertures involves using the time-varying relative dynamics for eccentric orbits first presented by Lawden [15] and applied to passive formation initialization in References [9,10]. The small correction for eccentricity is critical in determining the desired state to maintain periodic motion. It is clear from the figure that the desired state changes with time as the satellite formation orbits around the earth. Details of passive aperture initialization and desired state propagation for elliptical orbits are in References [10, 14].

The second issue in the formation control problem is which relative dynamics to use in the linear programming formulation. For the formation initialization maneuver, the dynamics are relative to the reference orbit used to determine the desired terminal state. The control problem is to determine the fuel-optimal control inputs and trajectory to achieve the desired terminal state at a fixed time. For formation-keeping, the dynamics are relative to a desired state that is changing with time, and an error box that represents the position tolerance for the formation-keeping is centred on the desired state (see Figure 5). In the case of a passive aperture design, the desired state and error box revolve around the reference orbit on the elliptical shape defined by the periodic relative motion. Reference [10] analyses the linear programming control approach

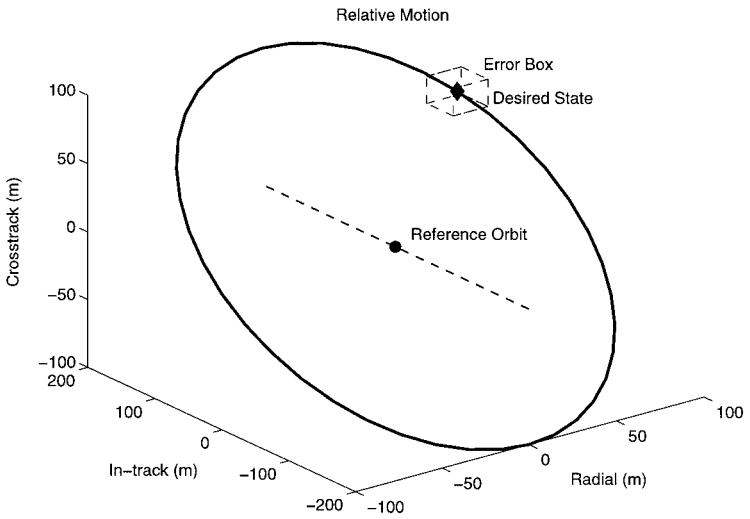

Figure 5. Motion of satellite relative to a reference orbit. The current position of the reference orbit is denoted with a circle, and the current desired relative position is denoted with a diamond. An error box is centred on the diamond.

using both the time-varying relative dynamics for eccentric orbits by Lawden and the time-invariant dynamics in Hill's equations. Note that the time-varying dynamics do not increase the actual size of the LP problem, but more computation is involved in the problem formulation. The nonlinear simulations in Reference [10] demonstrated that, for small eccentricities, the time-invariant Hill's relative dynamics could be used in the LP control problem with minimal increase in fuel cost. Hill's dynamics are sufficient because the control problems take place over short time scales, typically less than an orbit.

Several nonlinear simulations were performed using FreeFlyer^{TM} orbit simulator [13] in order to demonstrate the effectiveness of the LP control method for determining fuel optimal control for each of these particular maneuvers. The FreeFlyer^{TM} orbit simulator propagates the absolute states of both satellites. The simulator allows the option of including or excluding disturbances such as drag, lift, solar radiation pressure, and J_2. The simulator software interfaces with MATLAB^{TM}, where the control calculations are performed.

The simulation presented in the following sections involves a three satellite formation. The reference orbit, represented by a virtual satellite with properties similar to the average of the fleet, has a semi-major axis of 6900 km, inclination 35°, and eccentricity 0.005. The spacecraft begin with an initial in-track separation of 250 m. A formation initialization maneuver is executed to achieve a passive aperture formation that projects a 400×200 m ellipse on the orbital plane and oscillates with an amplitude of 100 m in the crosstrack direction. This aperture is maintained through formation-keeping for two days then the formation reconfigures to a second passive aperture with a projected in-plane ellipse of 1200×600 m and crosstrack amplitude of 300 m. The crosstrack motion is phased by 90° which causes the plane of the formation to rotate 90° from the previous aperture. All disturbances (J_2, drag, solar radiation

pressure, etc.) were included in all simulations, however, only differential drag was included in the LP control formulation.

Each satellite is modelled as an Orion spacecraft based on current specifications for the Orion–Emerald mission [6,40]. Each satellite has a mass of 45 kg, but they have slightly different ballistic coefficients, resulting in a differential drag disturbance. The satellite thrusters are restricted to provide a maximum acceleration of 0.003 m/s^2 and a minimum of 5×10^{-6} m/s^2. The maximum thrust corresponds to turning on the thruster for the full time-step. The minimum thrust is determined from a minimum impulse bit of 10 ms during the time-step. The relative dynamics for the satellites are discretized on a 5.4 s time-step. Lawden's time-varying equations are used to determine the desired state for each spacecraft, however Hill's equations are used in LP problem.

During each time-step in the dynamics the following sequence of events occur in FreeFlyer^{TM} and MATLAB^{TM}. The current absolute state in the ECI frame is passed from FreeFlyer to MATLAB. The states of each satellite are then converted from the ECI frame used by FreeFlyer to the local reference frame (radial, in-track, crosstrack) used in the control implementation. Each satellite has a position and velocity relative to the virtual satellite representing the reference orbit. The desired relative state of the each satellite is then determined based on the virtual satellite's true anomaly, eccentricity, and semi-major axis, and the individual satellite's formation phasing. These calculations use the homogenous solutions to the time-varying relative dynamics of Lawden (see Reference [10]). Depending on the type of maneuver in progress, any pre-existing plans, and the error state of the satellite, either the current step in an existing plan is implemented or a new plan is developed using linear programming. Further details on the appropriate control and plan development logic for each maneuver type are provided in the following sections. The control inputs from the plan, if required, are converted to small displacements and velocity changes using the time-changing dynamics. These relative state variables are transformed into the ECI frame and passed back to FreeFlyer. They are then added to the absolute state vector of the satellite after the input-free state propagation is performed by the FreeFlyer^{TM} software to give the state of each satellite at the beginning of the next time-step. The result is a real-time linear control in a complex nonlinear simulation environment.

To simplify the following discussion, the simulation details and results are discussed by maneuver type. The formation initialization and reconfiguration maneuvers are discussed first followed by the formation-keeping maneuvers. The discussion of each maneuver type includes details on the control problem formulation and implementation. This is followed by a discussion of the effects of sensor noise on each controller performance and methods of improving control.

6.1. Formation initialization and reconfiguration maneuvers

The formation initialization and reconfiguration control problem is to determine the fuel-optimal trajectory and required control inputs to move a fleet of spacecraft from the current states to some desired terminal states over a fixed time interval. Several quantities must be determined for the spacecraft maneuvers.

First, a desired final state must be determined. The desired final state is usually on a passive aperture that results in periodic relative motion between the satellites in the formation. The phasing between the satellites on the aperture is usually constrained, however the actual initialized position is not. In order to consider various final positions, the desired aperture is

discretized into a finite number of terminal positions. Each possible final formation can be described by a formation anomaly, which is a phasing from 0° to the first satellite on the ellipse and a formation order. The formation is the ordering of the satellites around the aperture from the 0° phase angle. The costs for each satellite to achieve each final state are combined to form a cost matrix which is used to determine the fuel-optimal configuration for the fleet. Details of the co-ordinator formulation are in Section 5. Discussion and simulation results for each part of the initialization or reconfiguration problem follow.

6.1.1. Fuel vs formation maneuver time (Figure 6)

As discussed in Section 4, the LP problem provides an efficient solution to the fuel optimization problem with a fixed end-time. However, the selection of this end-time can have a significant effect on the total fuel used. Consider the initialization maneuver described in Section 6 wherein the group of satellites start with an along track separation on a reference orbit and transfer to a closed-form aperture centred on the same reference orbit. In this optimization, the starting and terminal positions and velocities for each vehicle are known, and the optimal solution can be readily found using LP for a given end-time. Figure 6 plots the fuel used vs maneuver time for one of the spacecraft in the fleet. As shown, the fuel usage can be reduced by a factor of approximately two if the transfer time is increased from a quarter of an orbit to one orbit. However, increasing the maneuver time beyond one orbit does not further reduce the fuel usage.

The maneuver time can also be selected to minimize an auxiliary cost function that describes the desired weighting on the fuel/time trade-off,

$$J_{\text{aux}} = \|u\|_1 + \lambda t_{\text{f}} \tag{59}$$

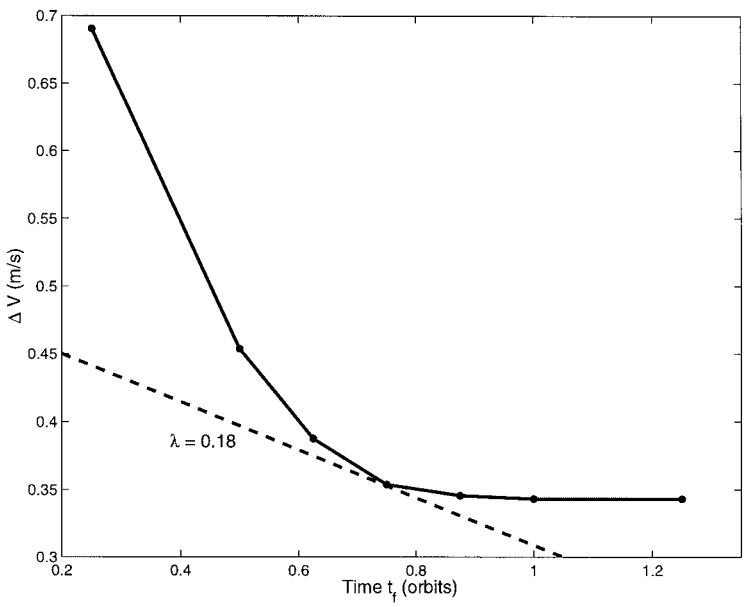

Figure 6. Fuel vs maneuver time for maneuver from a line to an aperture (200 m semi-major axis). With a relative weighting of $\lambda \approx 0.18$, the best maneuver time would be ≈ 0.75 orbits.

The lowest value of $J^{\star}_{\text{aux}}$ corresponds to the point with the normal, $R_{\text{N}} = [-\lambda, -1]^{\text{T}}$. Of course, there are typically many constraints on the length of the transfer/reconfiguration maneuvers. However, these LP optimizations provide an efficient means of investigating the impact of basic mission design questions such as the selection of an appropriate maneuver time for the formation reconfiguration.

6.1.2. Formation co-ordination

The formation co-ordinator discussed in Section 5 is used to determine the fuel-optimal trajectories for the initial maneuver from an in-track separation to a passive aperture. The formation co-ordination results in an optimum satellite order of $I_{o1} = [3\ 2\ 1]$ with a formation anomaly of 60° and a predicted $\Delta V = 0.520$ m/s. The result of using a simple choice for the final formation order ($I_1 = [1\ 2\ 3]$ with a 0° anomaly, i.e. vehicle 1 moves to location 1 on the target ellipse) is $\Delta V = 0.580$ m/s (a 10 per cent increase from the optimal solution case). Additional possible configurations could result in an increased fuel cost as high as 20 per cent.

Similar results were developed for the second formation maneuver. Maneuvering the formation into the same $I_1 = [1\ 2\ 3]$ configuration has a cost of $\Delta V = 2.743$ m/s. The co-ordination process was performed for the second maneuver to determine that a formation configuration of $I_{o2} = [2\ 3\ 1]$ (anomaly of 30°) has a slightly lower fuel cost of $\Delta V = 2.537$ m/s ($\approx$ 8 per cent less fuel than the I_1 case). An analysis of all possible configurations indicates that selecting a non-optimized final configuration for the fleet could result in fuel costs that are 5–25 per cent higher than the optimal for maneuvers of this type.

6.1.3. Simulation results (Figures 7–10)

No measurement noise—The first simulation implements the control scheme assuming knowledge of the satellite positions and velocities without noise/uncertainty. This corresponds to the ideal case and is used to demonstrate the extent to which LP can be used to generate fuel-optimal trajectories. Figures 7 and 8 show the initial maneuver to a closed-form ellipse and the second maneuver from one ellipse to another. The fuel used by each satellite for the maneuvers are shown in Table I. The actual fuel use in FreeFlyer agrees with the predictions by the co-ordinator for the initial maneuver (0.520 m/s), but differs slightly for the second maneuver (2.560 m/s). This small difference is a result of the satellite's deviation from the initial position and velocity that was used by the co-ordinator in the trajectory optimization.

Noise—A simulation was also performed to implement the control scheme with measurement noise included to add uncertainty in the knowledge of the relative positions and velocities of the satellites. The noise is modelled in the simulations as the true state vector plus a white noise component. An estimator is currently not used. The noise is restricted to a maximum amplitude of 2 cm for position and 1 mm/s for velocity as per current studies in GPS measurement noise [26,27]. Because the formation reconfiguration maneuvers are based on initial conditions that are uncertain, the satellite will not follow the desired trajectories.

Noise: LQR feedback control—One method of ensuring the satellite continues on the trajectory is to use feedback control to force the satellites to track the desired trajectory for the maneuvers. The desired position and velocity during the formation maneuver is determined for each satellite by simulating the response to the LP designed inputs. An error box is centred on the desired position for each satellite at each time-step during the maneuver. If the satellite is within the error box, no feedback control is applied, otherwise a simple linear quadratic regulator (LQR) is used to drive the satellite position to the desired position and hence back into

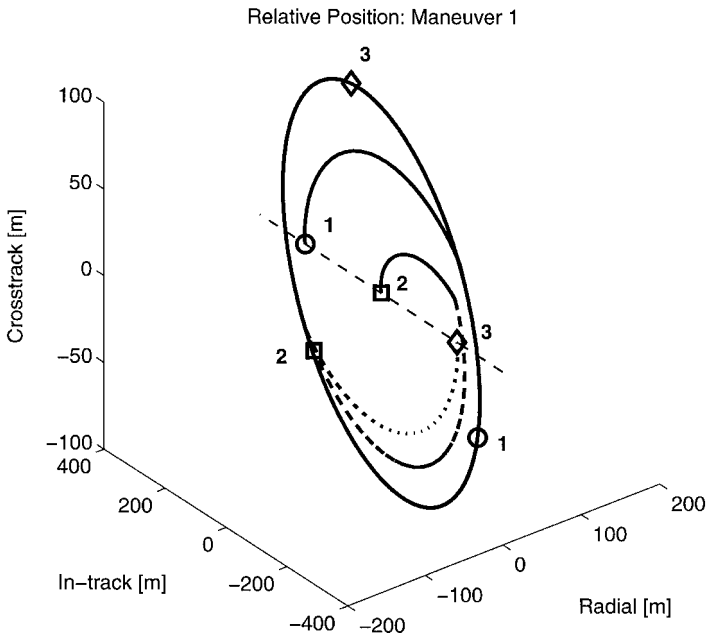

Figure 7. Reconfiguration from a line (250 m separation) to an aperture (200 m semi-major axis) followed by two days of formation-keeping. Feedforward control only.

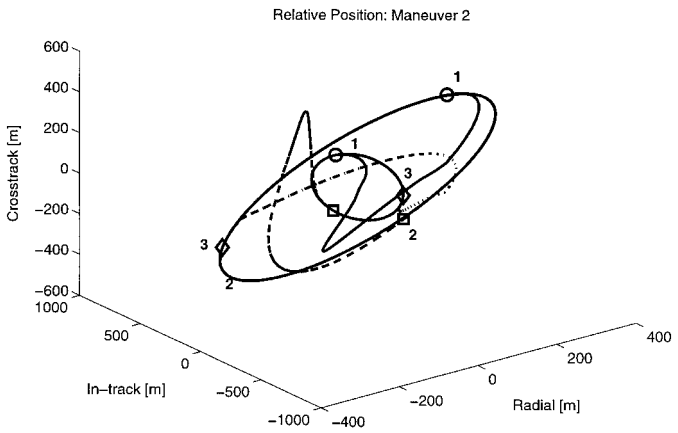

Figure 8. After 2 days (32 orbits) of formation-keeping, the fleet reconfigures to a new non-coplanar aperture (600 m semi-major axis). The fleet resumes formation-keeping at the new configuration.

the error box. The LQR control is used until the position state of the satellite returns back inside the error box. This feedback control is only applied when there are no scheduled feedforward control inputs.

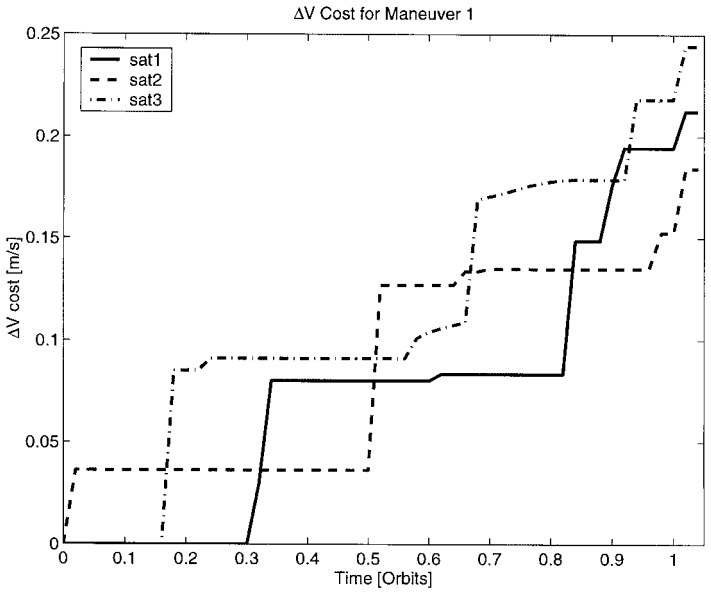

Figure 9. Total fuel (ΔV) used for the first reconfiguration maneuver. The total $\Delta V = 0.641$ m/s.

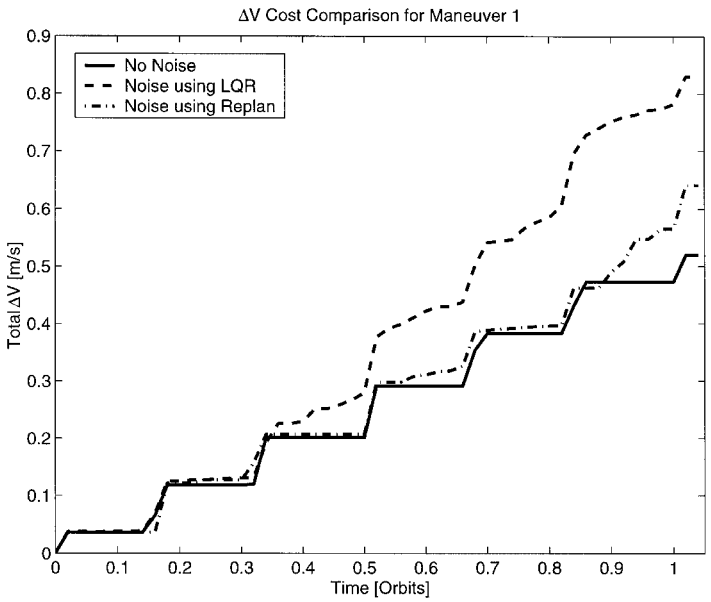

Figure 10. Total fuel (ΔV) comparison of using feedforward, feedforward/feedback LQR, and replanning for first reconfiguration maneuver. Total change in $\Delta V = 0.310$ m/s for feedback LQR and $\Delta V = 0.121$ m/s for replanning.

In this case, the results of the formation reconfiguration maneuvers are essentially the same as those shown in Figures 7 and 8. The fuel results are summarized in Table I. With errors in the initial conditions, the initial maneuver requires a $\Delta V = 0.830$ m/s, which corresponds to an extra 0.310 m/s (60 per cent increase) due to feedback control. The second maneuver requires an extra 0.360 m/s (15 per cent increase) for feedback control.

Noise: replan—Another method of completing the formation reconfiguration in the presence of measurement noise is by replanning over a reduced horizon during the maneuver. For this method, the desired position for the satellite during the maneuver is simulated using the designed inputs from the LP problem. An error box is centred on the desired position at each time-step. However, now when the error in position of the satellite exceeds the error box, a new plan is determined based on the current state. The new plan occurs over a plan length that is reduced by the number of time-steps executed up to that point. One advantage of this method is that, rather than tracking a trajectory based on incorrect initial conditions, a new trajectory is determined based on the current knowledge of the satellite state.

The simulations results for this method are summarized in Table I. Using the replanning method, the fuel cost with initial condition uncertainty for the initialization maneuver is only increased by 0.121 m/s (23 per cent increase) from the no noise case (approximately one-third of the fuel increase using LQR). The fuel increase for the formation reconfiguration is 0.074 m/s (3 per cent increase), which is again a significant improvement over the LQR result. A comparison of combined formation fuel cost for the initialization maneuver with and without uncertainty using the two methods described above is shown in Figure 10.

6.2. *Formation-keeping maneuvers*

For the formation-keeping maneuvers, the control is relative to the desired state for each spacecraft rather than the reference orbit. The desired relative state is differenced with the true relative state of the satellite to obtain the current *error state*. An error box that is centred on the desired position is used to determine if control action is required. The size of the error box is determined by the position tolerances permitted for the mission objective.

Table I. Fuel summary for reconfiguration maneuvers.

Maneuver	Fuel cost	Sat 1	Sat 2	Sat 3	Total
Initial move	Predicted				0.520 m/s
	No uncertainty	0.173 m/s	0.173 m/s	0.173 m/s	0.520 m/s
	Uncertainty-LQR	0.336 m/s	0.174 m/s	0.320 m/s	0.830 m/s
	Difference				0.310 m/s
	Uncertainty-replan	0.212 m/s	0.184 m/s	0.244 m/s	0.641 m/s
	Difference				0.121 m/s
Second move	Predicted				2.536 m/s
	No uncertainty	0.917 m/s	0.820 m/s	0.821 m/s	2.559 m/s
	Uncertainty-LQR	1.004 m/s	0.881 m/s	0.945 m/s	2.862 m/s
	Difference				0.303 m/s
	Uncertainty-replan	0.920 m/s	0.857 m/s	0.837 m/s	2.614 m/s
	Difference				0.055 m/s

Based on the position tolerance of 10 per cent of the baseline (100 m) specified by the TechSat-21 mission objectives [5], a 10 m in-track, 5 m radial, and 5 m out-of-plane box is used in these simulations.

In a typical implementation, each satellite is constrained to remain close (specified by the error box) to a desired location in the formation. When the satellite reaches the edge of the error box, the LP approach is used to design a trajectory that moves the satellite to a final position (e.g. near the centre or the far end of the box) while remaining within the error box and using a minimum amount of fuel. The terminal constraint is specified as in Equation (41). Figure 11 shows a trajectory that moves the satellite to within 1 m of the centre of the error box at the end of four orbits. Note that the satellite begins near the centre and drifts to the right under the differential drag. Figure 12 shows the control inputs used to generate the trajectory. Only inputs in the in-track direction were required to complete the maneuver, and all inputs occur at the beginning of the maneuver. Disturbances such as differential drag and differential J_2 can be included as additional inputs to the system dynamics as in Equation (22). With these inputs, the LP approach can be used to generate fuel-optimal trajectories for long-term formation-keeping that account for these disturbances. Differential drag can be modelled as a constant or sinusoidal input for each satellite, and its effect will depend on whether the satellite's drag is more or less than the average drag of the entire fleet (i.e. the satellite will tend to drift ahead or lag behind). The differential drag in this LP is modelled as a constant $\pm 0.5 \times 10^{-7}\ \mathrm{m/s^2}$ acceleration. This acceleration depends on the difference between the drag coefficient for each satellite and the average drag coefficient for the fleet.

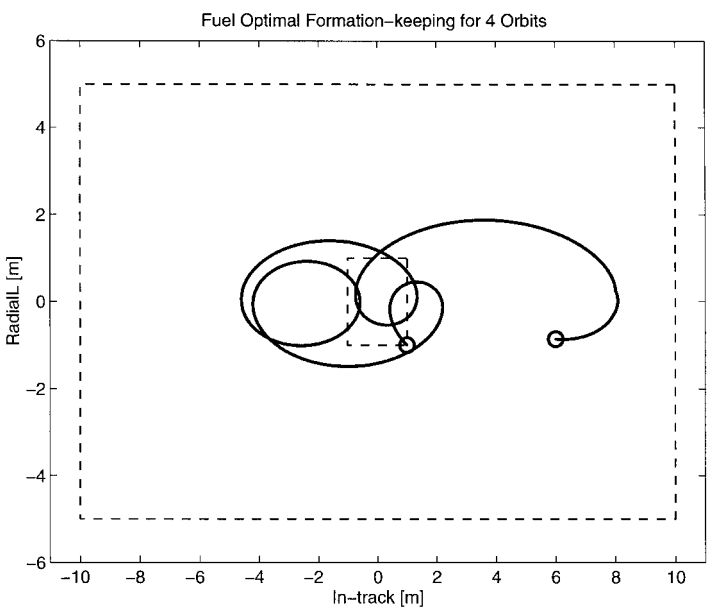

Figure 11. Planned trajectory for four orbits when initial conditions are known.

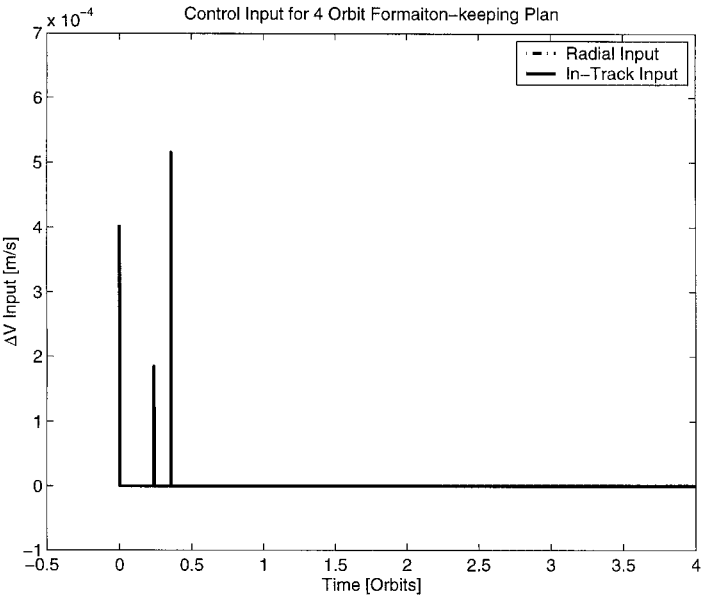

Figure 12. Control inputs for trajectory in Figure 11. No radial inputs were required.

6.2.1. Robust LP for initial condition uncertainty (Figures 13–15)

Any planned trajectory will rely heavily on the knowledge of the satellite's initial conditions. However, the initial relative positions and velocities must be measured and will be noisy. Note that a velocity uncertainty of 2 mm/s in the in-track direction results in approximately 30 m in-track position error after only one orbit. To examine this point further, consider a velocity uncertainty of ± 2 mm/s in the system described in the previous section. Figure 11 shows the trajectory for the control inputs designed for the nominal case. The inputs keep the satellite within the error box for four orbits and the path terminates near the centre. However, Figure 13 shows the response with perturbed velocity initial conditions (± 2 mm/s in-track, ± 2 mm/s radial). In this case, three of the trajectories violate the constraint box and two of the paths leave the box and never return.

Section 4.3 presents a modification to the LP algorithm that reduces sensitivity to the initial condition uncertainty by considering several different initial conditions. However, due to the large impact of the initial velocity errors, the length of the planning horizon must be reduced or the error box size must be increased. For the examples considered in this paper, the horizon was reduced to approximately one-quarter of an orbit and the terminal constraint was removed. Figure 14 shows the response to the four perturbed velocity initial conditions (and two additional cases) for a quarter orbit plan that was based on the nominal case. Note that four of the paths exit the error box. This is not surprising, as the LP was only designed for the nominal case. The control inputs from the robust LP were applied to the same set of initial conditions to generate the trajectories in Figure 15. Only four of these initial conditions were included in the

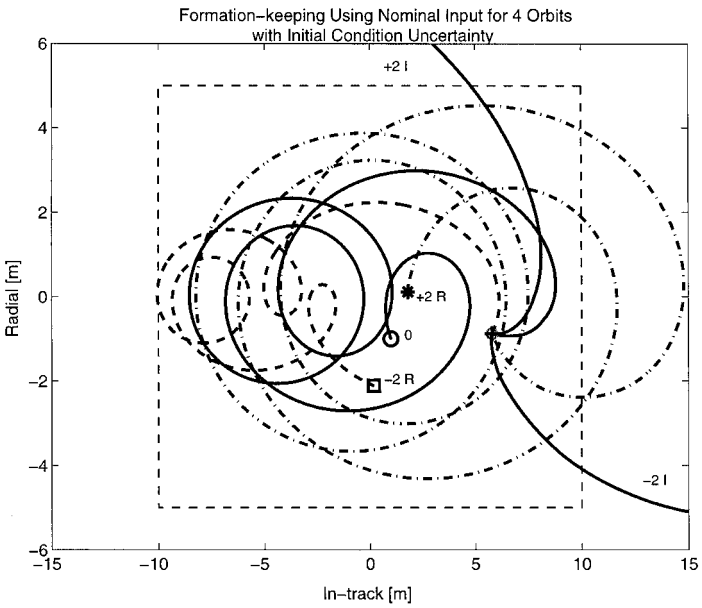

Figure 13. Trajectory followed using a nominal plan designed for four orbits without considering the initial condition uncertainties. The trajectories for ± 2 mm/s in-track error had final position errors of approximately ± 130 m.

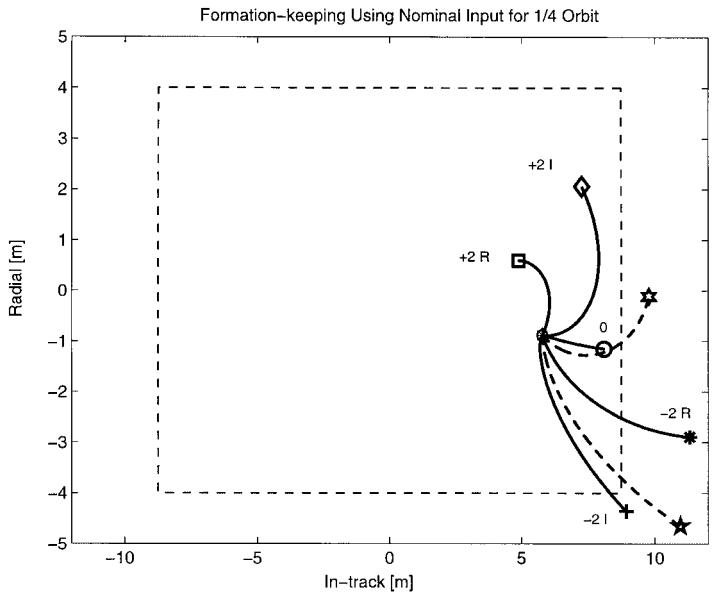

Figure 14. Trajectories for each of the five possible initial conditions using plan for nominal case. The pentagon and hexagon represent two additional cases within the uncertainty ellipsoid but not considered in the plan.

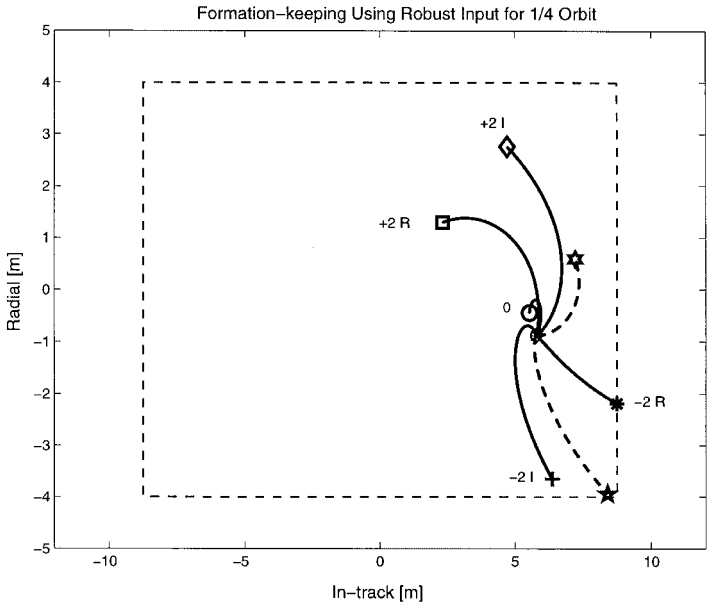

Figure 15. Trajectory followed using robust plan for each initial condition using robustified plan. The pentagon and hexagon represent two additional cases within the uncertainty ellipsoid but not considered in the plan.

LP design (labelled ones). However, as shown, all six trajectories remain within the box during this first quarter orbit.

The robustness to the initial condition uncertainty can be improved by considering many more initial conditions. This step is accomplished at the expense of calculating more **b** vectors, but the LP problem remains unchanged. The simulations in Section 6.2.2 consider 12 possible values of the initial conditions. However, when more initial velocity conditions are considered in the design, it can become very difficult to find feasible solutions to the LP problems. Further analysis of the effects of sensor noise on the formation-keeping control are available in Reference [30].

6.2.2. Simulation results (Figures 16–20)

No measurement noise—The position of one of the vehicles within the error box for formation-keeping is shown in Figure 16. An LP was used to generate inputs to maintain the satellite within the error box for half orbit time intervals and end within 1 m of the centre of the error box. Because the dynamics modelled in the LP are not exactly the same as those in the FreeFlyer simulation and J_2 was not included in the LP model, a shorter plan interval was required than when the plant dynamics are exactly known. The fuel use for formation-keeping during 32 orbits is shown in Figure 17. The formation-keeping for one satellite requires approximately $\Delta V = 12$ mm/s per orbit.

Noise: robust LP—A second simulation implements the control scheme with measurement noise included to add uncertainty in the knowledge of the relative positions and velocities of the satellites. The robust LP generates inputs that will keep the trajectory associated with the 'worst

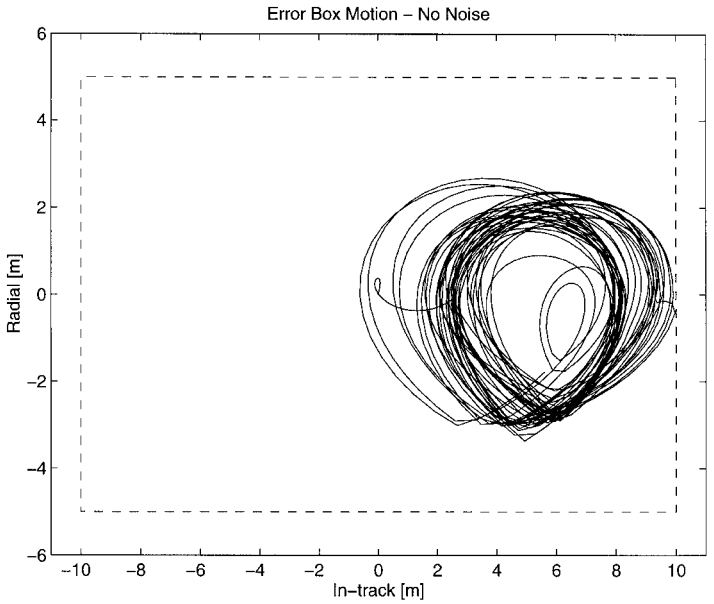

Figure 16. Typical in-plane error box motion of the spacecraft. No measurement noise used in the 2 day (32 orbit) simulation.

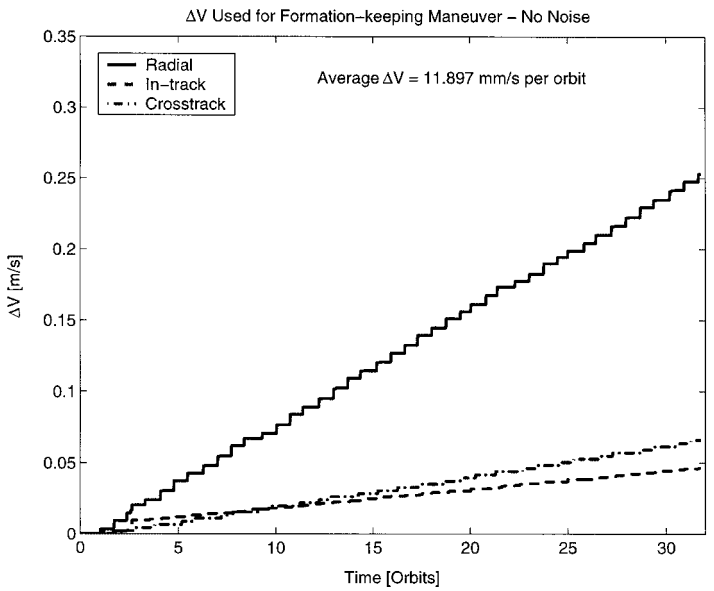

Figure 17. Fuel used to stay inside the error box for 2 days (32 orbits). LP plans designed for half an orbit.

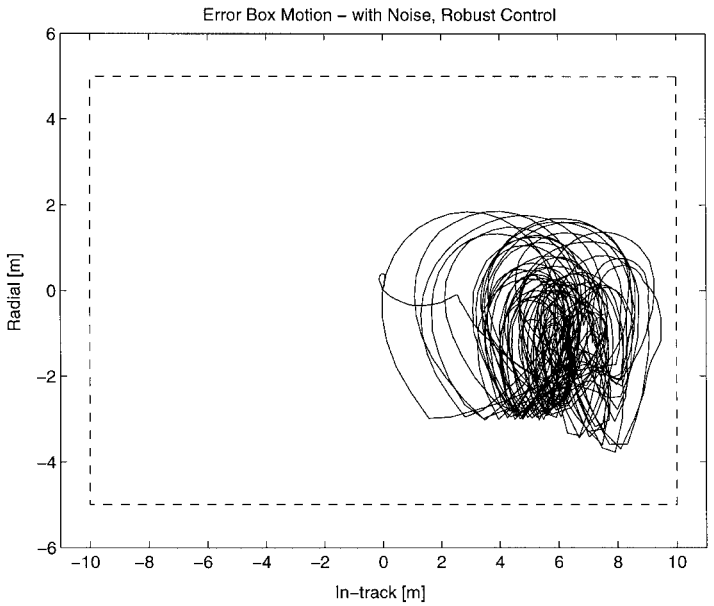

Figure 18. Typical in-plane error box motion of the spacecraft for 2 days (32 orbits).

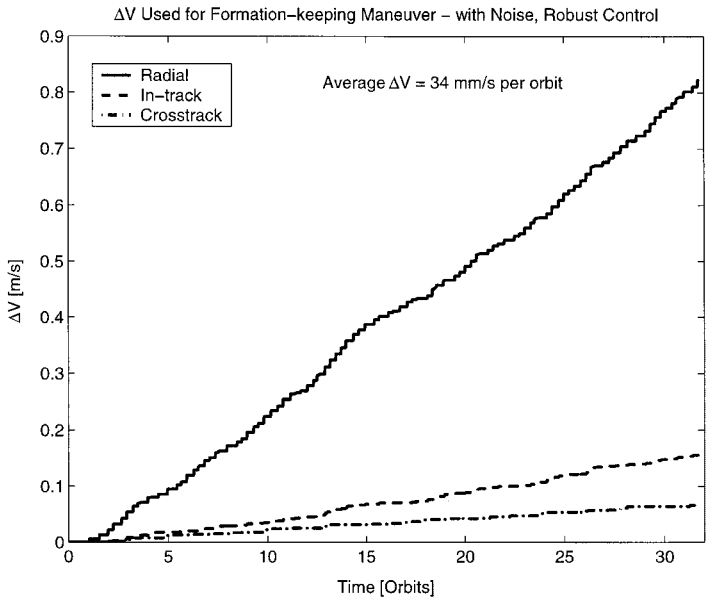

Figure 19. Fuel used for formation-keeping within the error box for 2 days (32 orbits). Robust LP plans designed for quarter orbit.

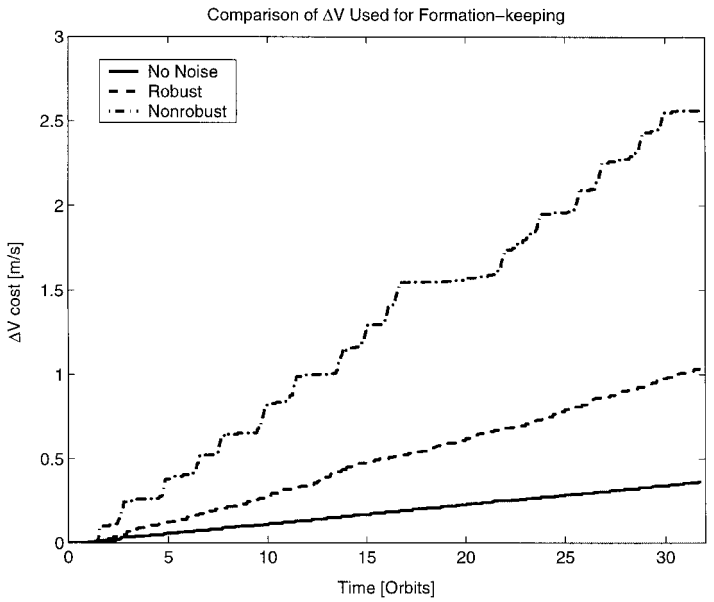

Figure 20. Comparison of fuel used for each type of formation-keeping control.

case' initial condition within the error box for the design horizon (one quarter of an orbit for these simulations). One example of the satellite position relative to the centre of the error box is shown in Figure 18 (compare with Figure 16). Note that, due to the initial condition uncertainty, the robust control input often applies ΔV commands in the opposite direction to the motion of the satellite, which results in abrupt changes of direction. As shown in the figure, the satellite always remains inside the error box despite only considering a finite number of possible initial conditions. The fuel use for the robust LP formation-keeping is shown in Figure 19. Formation-keeping using the robust LP requires approximately $\Delta V = 34$ mm/s per orbit for each satellite.

For comparison, a second simulation with the same noise level was performed using the standard LP approach (i.e. non-robust) to generate inputs for a quarter orbit. In this case, the formation-keeping required a $\Delta V = 70$ mm/s per orbit for one satellite. The increase in fuel is due to the inability of the non-robust plan to keep the satellite within the error box, which results in more frequent constraint violations and the need to replan more often. In fact, in this second simulation, the satellite exited the error box several times. A comparison of fuel cost for formation-keeping using LP with no uncertainty, the robust LP with uncertainty, and a non-robust LP with uncertainty is shown in Figure 20.

7. CONCLUSIONS

This paper presents fuel/time-optimal algorithms for a co-ordination and control architecture developed for distributed spacecraft systems. This architecture includes both the low-level

formation-keeping control and a high-level co-ordinator that designs trajectories to reconfigure the formation. The trajectory and formation-keeping optimization algorithms are based on the solutions of linear and integer programming problems. The result is a very flexible optimization framework that can be used off-line to analyse various aspects of the mission design and in real time as part of an onboard autonomous formation flying control system. The overall control approach is demonstrated using a realistic nonlinear simulation environment. The simulation results indicate that noise in the relative velocity measurements could play a crucial role in the fleet performance and/or fuel cost.

REFERENCES

1. Bauer FH, Hartman K, Bristow J, Weidow D, How JP, Busse F. Enabling spacecraft formation flying through spaceborne GPS and enhanced autonomy technologies. *ION-GPS '99*, *Proceedings of the 12th International Technical Meeting of the Satellite Division of the Institute of Navigation*, Nashville, TN, September 14–17, 1999 (*A01-27218 06-32*). Institute of Navigation: Alexandria, VA, 1999; 369–383.
2. Das A, Cobb R. TechSat 21—space missions using collaborating constellations of satellites. *Proceedings of AIAA/USU 12th Annual Conference on Small Satellites*, Utah State University, Logan, August 31–September 3, 1998. (*A99-10826 01-20*). Utah State University: Logan, UT, 1998.
3. Beichman CA. The terrestrial planet finder—the search for life-bearing planets around other stars. *Proceedings of Astronomical Interferometry Meeting*, Kona, HI, March 20–24, 1998. *Pt. 2* (*A98-40801 11-35*). Society of Photo-Optical Instrumentation Engineers: Bellingham, WA, (*SPIE Proceedings*, vol. 3350), 1998; 719–723.
4. Bauer F, Bristow J, Folta D. Hartman K, Quinn D, How J. Satellite formation flying using an innovative autonomous control system (AutoCon) environment. *Proceedings of AIAA Guidance*, *Navigation*, *and Control Conference*, New Orleans, LA, August 11–13, 1997, *Collection of Technical Papers*, *Pt. 2* (*A97-37001 10-63*). American Institute of Aeronautics and Astronautics: Reston, VA, 1997; 657–666.
5. Air Force Research Laboratory Space Vehicles Directorate. TechSat 21 factsheet page. http://www.vs.afrl.af.mil/factsheets/TechSat21.html(www.vs.afrl.af.mil/factsheets/TechSat21.html).
6. How J, Twiggs R, Weidow D, Hartman K, Bauer F. Orion—a low-cost demonstration of formation flying in space using GPS. *Proceedings of AIAA/AAS Astrodynamics Specialist Conference and Exhibit*, Boston, MA, August 10–12, 1998. *Collection of Technical Papers* (*A98-37348 10-13*). American Institute of Aeronautics and Astronautics: Reston, VA, 1998; 276–286.
7. Sedwick R, Miller D, Kong E. Mitigation of Differential Perturbations in Clusters of Formation Flying Satellites. *Proceedings of the AAS/AIAA Space Flight Mechanics Meeting*, Breckenridge, CO, February 7–10, 1999. *Pt. 1* (*A99-39751 10-12*). Univelt, Inc.: San Diego, CA (*Advances in the Astronautical Sciences*, vol. 102, pt. 1), 1999; 323–342.
8. Schaub H, Alfriend K. J_2 invariant relative orbits for spacecraft formations. In manuscript form, 1999.
9. Inalhan G, How J. Relative dynamics and control of spacecraft formations in eccentric orbits. *Proceedings of the Guidance*, *Navigation*, *and Control Conference and Exhibit*, Denver, CO, August 14–17, 2000. *Collection of Technical Papers*. American Institute of Aeronautics and Astronautics: Reston, VA, 2000.
10. Tillerson M, How J. Formation flying control in eccentric orbits. *Proceedings of the AIAA Guidance*, *Navigation*, *and Control Conference*, Montreal, Canada, August 6–9, 2001. *Collection of Technical Papers*. American Institute of Aeronautics and Astronautics: Reston, VA, 2001.
11. Robertson A, Inalhan G, How J. Formation control strategies for a separated spacecraft interferometer. *Proceedings of the 1999 American Control Conference*, vol. 6, San Diego, CA, June 2–4, 1999. (*A00-15511 02-63*). Institute of Electrical and Electronics Engineers: Piscataway, NJ, 1999; 4142–4147.
12. Robertson A, Inalhan G, How J. Spacecraft formation flying control design for the Orion mission. *Proceedings of the AIAA Guidance*, *Navigation*, *and Control Conference and Exhibit*, Portland, OR, August 9–11, 1999. *Collection of Technical Papers*, vol. 3 (*A99-36576 09-63*). American Institute of Aeronautics and Astronautics: Reston, VA, 1999; 1562–1575.
13. Perkins F. *Freeflyer User's Documentation*. AI Solutions: Lanham, Maryland, April 2000.
14. Inalhan G, Tillerson M, How J. Relative dynamics & control of spacecraft formations in eccentric orbits. *AIAA Journal of Guidance*, *Control and Dynamics*, January 2000, to appear.
15. Lawden D. *Optimal Trajectories for Space Navigation*. Butterworths: London, 1963.
16. Marec J. *Optimal Space Trajectories*. Elsevier Scientific: New York, 1979.
17. Bate R, Mueller D, White J. *Fundamentals of Astrodynamics*. Dover Publications Inc.: New York, 1971.
18. Chobotov V. *Orbital Mechanics* (2nd edn), AIAA Educational Series. AIAA: New York, 1996.
19. Franklin G, Powell J, Workman M. *Digital Control of Dynamic Systems* (3rd edn). Addison-Wesley: Reading, MA, 1998.

20. Tillerson M, How J. Advance guidance algorithms for spacecraft formation flying. *2002 American Control Conference*, Anchorage, AK, May 8–10, 2002. Institute of Electrical and Electronics Engineers: Piscataway, NJ, 2002, submitted.
21. Boyd S, El Ghaoui L, Feron E, Balakrishnan V. Linear matrix inequalities in system and control theory. *Studies in Applied Mathematics*, vol. 15. SIAM: Philadelphia, 1994.
22. Boyd S, Vanderberghe L. Convex optimization. In *manuscript form*, http://www.stanford.edu/class/ee364/reader.ps(www.stanford.edu/class/ee364/reader.ps), 1999.
23. Coleman T, Branch M, Grace A, *Optimization Toolbox for use with Matlab*. The Mathworks Inc., January 1999.
24. See www.cplex.com
25. See http://www-fp.mcs.anl.gov/otc/Tools/PCx/(www-fp.mcs.anl.gov/otc/Tools/PCx)
26. Busse F, How J, Simpson J, Leitner J. PROJECT ORION-EMERALD: carrier differential GPS techniques and simulation for low earth orbit formation flying. Presented at the *IEEE Aerospace Conference*, March 10–17, 2001.
27. Busse F, Inalhan G, How J. Project Orion—carrier phase differential GPS navigation for formation flying. *Guidance and Control 2000*, *Proceedings of the Annual AAS Rocky Mountain Conference*, Breckenridge, CO, February 2–6, 2000 (*A00-41276 11-12*). Univelt. Inc.: San Diego, CA, *Advances in the Astronautical Sciences*, vol. 104, 2000; 197–212.
28. Grocott S, How J, Miller D, MacMartin D, Liu K. Robust control design and implementation on the middeck active control experiment. *AIAA Journal of Guidance, Control, and Dynamics* (0731-5090) 1994; 17(6) 1163–1170.
29. Bryson A, Mills R. Linear-quadratic-Gaussian controllers with specified parameter robustness. *AIAA Aerospace Sciences Meeting and Exhibit*, 32nd, Reno, NV, January 10–13, 1994. *AIAA Paper* 94-0002, *AIAA Journal of Guidance, Control, and Dynamics* (0731-5090) 1998; 21(1):11–18.
30. How J, Tillerson M. Analysis of the impact of sensor noise on formation flying control. *Proceedings of the 2001 American Control Conference*, Arlington, VA, June 25–27, 2001. Institute of Electrical and Electronics Engineers: Piscataway, NJ, 2001.
31. Ben-Tal A, Nemirovski A, Robust solutions of uncertain linear programs via convex programming. *Technical Report*, Faculty of Industrial Engineering and Management, Technion, iew3.technion.ac.il/Labs/Opt/1997.
32. Clearwater S. *Market-Based Control, a Paradigm for Distributed Resource Allocation*. World Scientific: Singapore, 1996.
33. Sedwick R, Hacker T, Miller D. Optimum aperture placement for a space-based radar system using separated spacecraft interferometry. *Proceedings of the AIAA Guidance, Navigation, and Control Conference and Exhibit*, Portland, OR, August 9–11, 1999. American Institute of Aeronautics and Astronautics: Reston, VA, 1999.
34. Floudas C. *Nonlinear and Mixed-Integer Programming—Fundamentals and Applications*. Oxford University Press: Oxford, 1995.
35. Williams H, Brailsford S. Computational logic and integer programming. In *Advances in Linear and Integer Programming*, Beasley JE (ed.). Clarendon Press: Oxford, 1996; 249–281.
36. Schouwenaars T, DeMoor B, Feron E, How J. Mixed integer programming for safe multi-vehicle cooperative path planning. Presented at the *European Control Conference*, 2001.
37. Richards A, Schouwenaars T, How J, Feron E. Spacecraft trajectory planning with collision and plume avoidance using mixed integer linear programming. *AIAA Journal of Guidance, Control and Dynamics*, October, 2001, submitted.
38. Kay M, *Logistics and Facilities Planning Toolbox*. Version 1.3, August 2000. Available at www.ie.ncsu.edu/kay/matlog/Contents.htm
39. Burkard R, Cela E. Linear assignment problems and extensions. In *Handbook of Combinatorial Optimization*, Du Z, Pardalos P (eds). Kluwer Academic Publishers: Dordrecht, 1999; 75–149.
40. Ferguson P, Busse F, Engberg B, How J, Tillerson M, Pohlman N, Richards A, Twiggs R. Formation flying experiments on the Orion–Emerald mission. *Proceedings of AIAA Space 2001 Conference*, *AIAA paper 2001-4688*.

